Chapter 4
Cell Locomotion in One Dimension

Pierre Recho and Lev Truskinovsky

4.1 Introduction

The ability of cells to self-propel is essential for most biological processes: in the early life of an embryo, stem cells move to form tissues and organs, during the immune response, leukocytes migrate through capillaries to attack infections and collective motion of epithelial cells is necessary for wound healing. While the molecular and biochemical basis of cell motility is basically known, the underlying mechanical theory of active continuum media is still under development [3, 23, 34, 39, 55, 71, 102, 118, 125, 168].

At a rather schematic level, sufficient for our purposes, a cell can be viewed as an elastic 'bag' whose interior is separated from the exterior by a bi-layer lipid membrane. The membrane is attached from inside to a cortex—an active muscle-type layer maintaining the cell's shape. The interior is filled with a passive medium, the cytosol, where all essential cell organelles are immersed. The active machinery inside the cytosol, ensuring self-propulsion, resides in the cytoskeleton: a perpetually renewed network of actin filaments that is cross-linked by myosin motors while being transiently attached to the cell exterior through adhesion proteins. The main active processes in the cytoskeleton are: the non-equilibrium polymerization of actin fibers, the relative sliding of actin fibers induced by myosin motors and the active bonding of trans-membrane proteins to viscous or elastic substrate [5, 23, 66, 102, 105].

P. Recho (✉)
Mathematical Institute, University of Oxford, Woodstock Road, Oxford OX26GG, UK
e-mail: recho@maths.ox.ac.uk

L. Truskinovsky
LMS, CNRS-UMR 7649, École Polytechnique, Route de Saclay, 91128 Palaiseau, France
e-mail: trusk@lms.polytechnique.fr

I.S. Aranson (ed.), *Physical Models of Cell Motility*, Biological and Medical Physics, Biomedical Engineering, DOI 10.1007/978-3-319-24448-8_4

The elementary mechanisms responsible for the steady crawling of keratocytes, flattened cells with fibroblastic functions that will be our main object of study, have been identified [2, 15, 16, 44, 65, 102, 127, 146, 160]. Like most other eukaryotic cells, they self-propel by advancing the front and retracting the rear. The advance starts with protrusion through active polymerization in the frontal area of the cell (the lamellipodium) with a simultaneous formation of adhesion clusters at the advancing edge. After the adhesion of the protruding part of the cell is secured, the cytoskeleton contracts due to activity of myosin motors. The contraction leads to detachment at the rear and disassembly of the actin network through de-polymerization.

It is usually assumed that active polymerization ensuring protrusion can be described as the work of spatially distributed 'pushers', generating positive force couples, while active contraction can be viewed as an outcome of the mechanical action of distributed 'pullers', responsible for negative force couples. One of our main goals will be to show that the relative roles of pushers and pullers in cellular motility may be interchangeable and tightly linked to the task to be performed, see also [33, 95, 124, 132, 144]. The active side of the reversible adhesion of adhesive patches (focal adhesions) is understood insufficiently and we treat them as passive viscous binders whose spatial distribution may be regulated actively [52].

The three main components of the motility mechanism (polymerization, contraction and adhesion) depend upon continuous supply of energy provided by the ATP hydrolysis. They also require intricate regulation by complex signaling pathways involving chemical and mechanical feedback loops and the implied synchronization allows the cell to move with a relatively stable shape and velocity [13, 152]. While the general crawling mechanisms described above can support non-stationary translocation of the cell body [6, 12, 93], in this chapter we focus exclusively on the study of steady motility modes and will deal, outside transients, with cell fragments advancing at a constant velocity.

A variety of multi-scale simulation approaches targeting various cell motility mechanisms can be found in the literature, see the reviews in [14, 34, 102, 120, 152, 163]. Among them, prominent role is occupied by continuum mechanical models, although the underlying rheological assumptions may be rather diverse. Thus, in some models, the cytoskeleton is viewed as a highly viscous active *fluid* moving through a cytoplasm by generating internal contractile stresses [7, 63, 77, 109]. In other models, the cytoskeleton is represented as an active gel whose polar nature is modeled in the framework of the theory of *liquid crystals* [28, 71, 73, 75, 82, 118]. The active gel theory approach has been quite successful in reproducing various sub cellular structures observed in vivo [46, 47, 49, 134] and we basically follow it in this chapter albeit without an explicit reference to local orientational order. At sufficiently fast time scales, the cytoskeleton can be also modeled as an active *solid* with highly nonlinear scale-free rheology [24, 116]. The range of rheological models compatible with mechanical behavior of cytoskeleton reflects the incredible adaptability of this active medium and mirrors the variety of different motility modes in disparate types of cells.

In addition to bulk rheology, various surface elements of the motility machinery have been subjected to focused studies. It was shown that in some cases the plasmic membrane with its attached cortex can be viewed as a passive elastic surface and modeled by phase field methods allowing one to pass smoothly through topological transitions [55, 153, 163]. In other cases, the membrane may also play an active role, for instance, an asymmetric distribution of channels on the surface of the membrane can be responsible for a particular mechanism of cell motility relying on variation of osmotic pressure [147]. Another type of activity is associated with muscle-type contractions in the cortex that play an important role in blebbing [139, 151] and mitosis [133, 156]. An important role of active feedback between the shape of a crawling cell and the diffusion of pushers along the plasma membrane, was emphasized in [3]. While most models assume that the cell membrane interacts with the exterior of the cell through passive viscous forces, active dynamics of adhesion complexes has recently become an area of intense research driven in part by the finding of a complex dependence of the crawling velocity on the adhesive properties of the environment [43, 44, 52, 88, 89, 107, 129, 138, 168].

The account of these and other relevant factors, including realistic geometry, G-actin transport, Rac/Rho-regulation, etc., has led to the development of rather comprehensive models of cell motility that are adequate not only qualitatively but also quantitatively and can already serve as powerful predictive tools, see for instance [14, 48, 55, 91, 131, 141, 153, 166] and other chapters of this book. However, a physical understanding of the separate roles played in various macroscopic manifestations by individual active components of the self-propulsion machinery and the appreciation of the associated competition and cooperation between different 'players' is usually obscured by geometrical and bio-chemical complexity of such models and remain hidden behind opaque computational schemes [48, 63, 141, 152, 163, 165, 166, 169].

To bring some transparency into the interplay between contraction, protrusion and adhesion and to develop the associated intuition, we overview in this chapter a set of deliberately simplified models of lamellipodial cell motility allowing one to achieve analytical results without sacrificing the main effect which each model is intended to illustrate. All these models involve one-dimensional projection of the complex intra-cellular dynamics on the direction of locomotion.

More specifically, we assume that the motor part of a crawling eukaryotic cell can be viewed as a one-dimensional continuum layer. The two free boundaries representing the front and the rear of the moving fragment are the places where the external fluxes can operate and the external loads can be applied. In particular, we suppose that actin treadmilling can take place only on these boundaries and that it can be modeled as an influx of mass at the front boundary and its disappearance at the rear boundary. The actomyosin cytoskeleton is modeled as an active gel and active contraction is represented by a spatially inhomogeneous pre-stress [83]. Adhesion is treated as spatially inhomogeneous viscous friction [48, 61, 75, 86, 131, 141].

In pursuit of analytic transparency, we decouple the momentum balance equation from the mass transport equation by assuming infinite compressibility of the

cross-linked actin network [75, 131]. The density of motors is either assumed to be constant or modeled by an advection-diffusion equation where the advection is due to the flow of actin. To ensure that the crawling cell maintains its size, we introduce a phenomenological cortex/osmolarity mediated quasi-elastic interaction between the front and the back of the self-propelling fragment [11, 12, 49, 93]; a comparison of such mean field elasticity with more conventional bulk elasticity models can be found in [122]. Similar coupling between the front and the rear of the fragment may have an active origin as well resulting from different rates of polymerization and de-polymerization at the extremities of the lamellipodium [50].

Different effects are emphasized in the three sections of this review and the corresponding minimal systems of equations, capable of capturing the desired effects, are adjusted accordingly. In all three sections our goal is to provide evidence that individual active mechanisms can either act separately or have to be coordinated in order to ensure the required performance.

In the first section we focus on active contraction while maximally simplifying adhesion and fully neglecting active protrusion. We build upon the observation that motility initiation in keratocytes may be triggered by raising the contractility of myosin [40, 92, 114, 159, 161, 167]. It is also known that cells may self-propel by contraction only [76]. By limiting our attention to 'pullers', we confront the existing theories of polarization and motility that place the main emphasis on 'pushers' and link motility initiation with active treadmilling and protrusion. Mathematically, our one-dimensional model reduces to a dynamical system of a Keller–Segel-type, however, in contrast to its chemotaxic analog, the nonlocality in this system which we call *autotaxis* is due to mechanical rather than chemical feedback. If compared with previous studies of Keller–Segel-type problems, our setting is complicated by the presence of free boundaries equipped with Stefan type boundary conditions. The model provides compelling evidence that both, the initiation of motility, associated with polarization, and its arrest, associated with re-symmetrization, may be fully controlled by the average contractility of motor proteins.

While contraction is crucial for pulling the organelles, protrusion is known to be the main mechanism of pushing [74]. In the second section we shift our focus to protrusion while maximally simplifying the description of contraction. More specifically, we assume that motor concentration is time independent and spatially homogeneous and keep adhesion passive. Our main result is that the roles of protrusion and contraction as the dominant mechanism of self-propulsion may by interchangeable depending on the character of the mechanical task performed by the cell. We identify a macroscopic signature of the dominance of each of the two mechanisms by demonstrating that the force-velocity relation associated with pushing is necessarily concave while pulling-dominated force-velocity relation may be convex-concave with an interval of negative mobility.

Finally, in the third section we mainly focus on active adhesion allowing it to optimally accommodate the dominating driving mode. We take an inverse engineering approach and use as optimality criterion the maximization of the overall velocity. For the given strength of protrusion, we prescribe the average level of contractile activity, and then search for the optimal internal distribution of contractile and

adhesive units. Our analysis of the ensuing variational problem demonstrates that radically different distributions of focal adhesions are most favorable depending on the domineering active mechanism of self-propulsion. Thus, for contraction-dominated motility, focal adhesions have to cooperate with pullers which end up localizing at the trailing edge of the cell while for protrusion-dominated motility they must conspire with pushers which concentrate at the leading edge of the cell. Both types of crawling mechanisms have been observed experimentally.

4.2 Contraction

As we have already mentioned, the problem of finding the mechanism of motility initiation is most commonly addressed in the framework emphasizing active polymerization [17, 32, 41, 64, 103, 135]. With such emphasis on 'pushers', spontaneous polarization was studied by Callan-Jones et al. [30], John et al. [74], Hawkins et al. [60], Hawkins and Voituriez [58], Doubrovinski and Kruse [48], and Blanch-Mercader and Casademunt [20]. In [10, 169] and [168], polarization was interpreted as a result of an inhomogeneity of adhesive interactions. Yet another group of authors successfully argued that cell polarity may be induced by a Turing-type instability [8, 70, 104, 157]. Such a diversity of modeling approaches is, of course, a manifestation of the fact that very different mechanisms of motility initiation are engaged in cells of different types.

The experimental evidence that contraction may be the leading factor behind the polarization of keratocytes has been broadly discussed in the literature. It was realized that active contraction creates an asymmetry-amplifying positive feedback because it causes actin flow which in turn carries the regulators of contraction [4, 14, 81, 124, 133]. In constrained conditions such autotaxis generates peaks in the concentration of stress activators (myosin motors) [22, 67] and this patterning mechanism was used, for instance, to model polarization induced by angular cortex flow [59, 61]. Closely related heuristic models of the Keller–Segel type [112] employing essentially the same physical mechanism of instability (autotaxis) and also describing symmetry breaking and localization were independently proposed in [31, 80]. In all these models, however, the effect of contraction (pullers) was obscured by the account of other mechanisms, in particular, polymerization induced protrusion (pushers), and the focus was on generation of internal flow and the resulting pattern formation, rather than on the problem of ensuring steady translocation of a cell.

More recent models of contraction-induced polarization relying on splay instability in an active gel were proposed in [55, 152, 153]. In these model, however, 'pushers' were not the only players, in particular, polarization was induced by a local phase transition from non-polar to polar gel. In a closely related paper [29], the motility initiation was attributed to a contraction-induced instability in a poro-elastic active gel permeated by a solvent. Here again the non-contractile active mechanism was involved as well and therefore the domineering role of contraction could not be made explicit.

A question intimately related to the problem of motility initiation is how the resulting steady translocation of a cell can be halted. Several computational models provided an indication that the two phenomena are related and that motility initiation and motility arrest may emerge from a re-entrant behavior of the same branch of motile regimes [55, 80, 124, 153]. However, it is still not clear whether motility initiation and motility arrest can be both fully contraction-driven. To address this issue we present in this section an analytically tractable one-dimensional model which answers the question positively and shows that the increase of contractility may cause not only polarization but also re-symmetrization.

Following previous work, we exploit the Keller–Segel (autotaxis) mechanism, but now in a free boundary setting. In contrast to most previous studies, our contraction driven translocation of a cell is caused exclusively by the internal flow generated by molecular motors (pullers) and no other active agents are involved, see also [124, 125]. While most of the elements of the proposed model have been anticipated by the comprehensive computational approaches, e.g. [131], it was previously not apparent that the initiation of motility, the steady translocation, the re-symmetrization and the arrest of motility can be all captured already in such a minimal model.

On the mathematical side, we show that the increase of contractility beyond a well defined threshold leads to a bifurcation from a static symmetric solution of the governing system of equations (of Keller–Segel type) describing non-motile cell to an asymmetric traveling wave (TW) solution describing steadily moving cell. While several TW regimes are available at the same value of parameters, we show that stable TW solutions localize motors at the trailing edge of the cell in agreement with observations [40, 92, 114, 159, 161, 167]. Moreover, we show that if adhesion with the extra-cellular substrate is sufficiently low, the increase of motor-induced contraction may induce transition from the steady state TW solution back to a static solution. This re-symmetrization transition, leading to the motility arrest, can be directly associated with the behavior of keratocytes prior to cell division [84, 85, 145] and our model shows that such a re-entrant behavior can be ensured exclusively by ‘pullers’ without any engagement of either active protrusion or liquid crystal elasticity.

4.2.1 A Toy Model

Our point of departure is a conceptual model elucidating the mechanism of contraction-driven crawling and emphasizing the role of symmetry breaking in achieving the state of steady self propulsion.

Recall that in crawling cells, the ‘motor part’ containing contracting cytoskeleton (lamellipodium), is a thin active layer located close to the leading edge of the cell, see Fig. 4.1. We assume that all mechanical action originates in lamellipodium and that from the mechanical viewpoint the rest of the cell, including the nucleus, can be interpreted as cargo. The main task will be to develop a model of freely moving

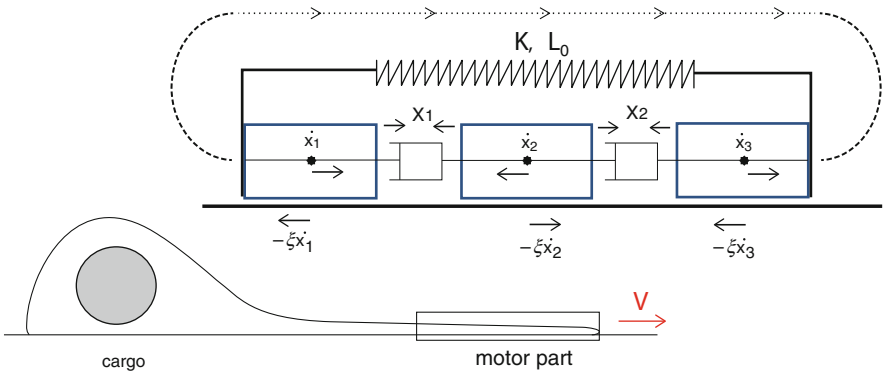

Fig. 4.1 Conceptual discrete model of the motility mechanism in a crawling keratocyte cell

lamellipodium which we schematize as a segment of active gel in viscous contact with a rigid background. The actin network inside the gel is contracted by myosin motors which leads to an internal flow opposed by the viscous interaction with the background. The unidirectional flow is a result of the asymmetry of contraction that ultimately propels the cell.

The simplest model elucidating this mechanism involves three rigid blocks of size l_b placed in a frictional contact with a rigid support, characterized by the viscous friction coefficient ξ. The neighboring blocks are connected by *active pullers* (force dipoles) exerting contractile forces. The long range signaling ensuring the control of cell volume is modeled by a linear spring with stiffness k connecting the first and the last block. To regularize the problem we place in parallel with contractile elements additional *dashpots* characterized by the viscosity coefficient η.

In the absence of inertia, we can write the force balance equations for our system in the form

$$\begin{aligned} -l_b\xi\dot{x}_1 + k\tfrac{x_3-x_1-L_0}{L_0} + \chi_1 - \eta\tfrac{\dot{x}_1-\dot{x}_2}{l_b} &= 0 \\ -l_b\xi\dot{x}_2 - \chi_1 + \chi_2 - \eta\tfrac{\dot{x}_2-\dot{x}_1}{l_b} - \eta\tfrac{\dot{x}_2-\dot{x}_3}{l_b} &= 0 \\ -l_b\xi\dot{x}_3 - k\tfrac{x_3-x_1-L_0}{L_0} - \chi_2 - \eta\tfrac{\dot{x}_3-\dot{x}_2}{l_b} &= 0, \end{aligned} \tag{4.1}$$

where $x_1(t), x_2(t), x_3(t)$ are the current positions of the blocks and L_0 is the reference length of a linear spring. This spring describes the membrane-cortex 'bag' around the lamellipodium allowing the inhomogeneous contraction to be transformed into a protruding force. We assume that polarization has already taken place and therefore the contractile force dipoles $\chi_1 \geq 0$ and $\chi_2 \geq 0$ acting between the two pairs of blocks are not the same $\chi_1 \neq \chi_2$. The polarization itself requires additional constructs and will be addressed later.

The system (4.1) can be rewritten as three decoupled equations for the length of our active segment $L(t) = x_3(t) - x_1(t)$, its geometric center $G(t) = (x_3(t) + x_1(t))/2$ and the position of a central block $x_2(t)$ representing the internal flow:

$$\begin{aligned} -l_b\xi(1+l_0^2/l_b^2)\dot{L} &= \chi_1+\chi_2+2k(L/L_0-1)\\ 2l_b\xi(1+3l_0^2/l_b^2)\dot{G} &= \chi_1-\chi_2\\ -l_b\xi(1+3l_0^2/l_b^2)\dot{x}_2 &= \chi_1-\chi_2. \end{aligned} \tag{4.2}$$

Here $l_0 = \sqrt{\eta/\xi}$ is the hydrodynamic length scale which will ultimately play the role of a regularizing parameter. The first equation shows that the length is converging to a steady state value:

$$L = L_0(1-(\chi_1+\chi_2)/(2k)).$$

Notice that in order to avoid the collapse of the layer due to contraction, it is necessary to ensure that the spring has sufficiently large stiffness $k > (\chi_1+\chi_2)/2$. We also observe that independently of the value of the evolving length $L(t)$, the velocity of the geometrical center of our train of blocks V is always the same

$$V = \dot{G} = \frac{\chi_1-\chi_2}{2l_b\xi(1+3l_0^2/l_b^2)}. \tag{4.3}$$

One can see that this mechanical system can move as a whole only if $\chi_1 \neq \chi_2$. This emphasizes the crucial role played in cell motility by the inhomogeneity of contraction. The origin of the implied gradients and the mechanism allowing the cell to maintain the inhomogeneity, will be addressed already in the continuum setting.

We observe that the middle block moves in the direction opposite to the motion of the center of the system with a constant velocity $\dot{x}_2 = -2V$. Therefore, it takes a finite time $\sim L/(3V)$ for the central block to collide with the block at the rear and additional assumptions are needed to extend the dynamics beyond the collision point.

To model circulation (turnover) of the cytoskeleton in a one-dimensional setting, we assume that while the flow is continuous along the contact surface, the cytoskeleton disintegrates into small pieces (actin monomers) at the trailing edge and reintegrates at the leading edge. This assumption allows us to close the treadmilling cycle, even though the details of the discontinuous part of the cycle, involving both reaction and an almost frictionless transport of monomers, will not be resolved by the model. The reverse flow will be replaced by instantaneous jumps maintaining the overall mass balance. We also neglect the active propulsion on the frontal boundary due to growth of the network.

More specifically, we assume that as a result of each collision a block at the rear is instantaneously removed from the chain and at the same time an identical block is added at the front. In other words, each (equilibrium) de-polymerization event at the rear is matched by an (equilibrium) polymerization event at the front. Essentially, we suppose that at the time scale of frictional (continuous) dynamics the reverse transport of monomers takes place instantaneously: we implicitly assume the existence of a stationary gradient of chemical potential of actin monomers and of a large pool of monomers ready to be added to the network at the front as soon as one of them is released at the rear.

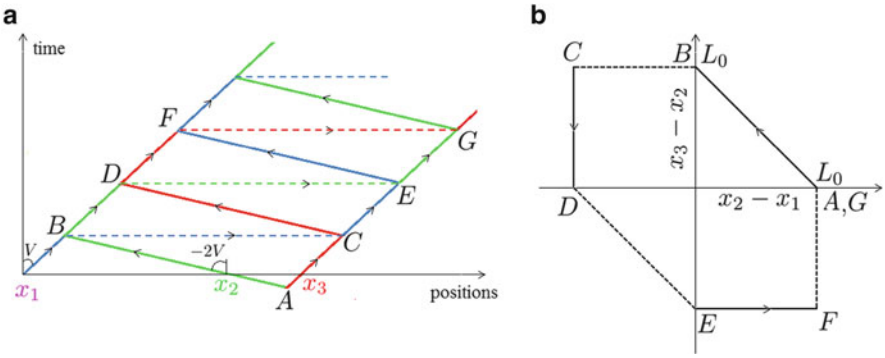

Fig. 4.2 (**a**) Schematic representation of the motion of individual particles (blocks) forming the motor part of a crawler in a steady state regime (three particle case). Trajectories in space time coordinates of the particles x_1 (*magenta*, *OBCEF*), x_2 (*green*, *ABDEG*) and x_3 (*red*, *ACDFG*); *dashed lines* show the jump parts of the crawling cycle. Continuous flows have to overcome friction while the jumps are assumed to be friction free. (**b**) A closed loop constituting one full stroke in the parameter space $(x_2 - x_1, x_3 - x_2)$. The time of one full stroke (A to G) is $T_s = L/V$ and the distance traveled by the crawler per stroke is $VT_s = L$

The structure of the resulting stroke in the t, x plane and in the $x_2 - x_1, x_3 - x_2$ plane is shown in Fig. 4.2. One can see that each block maintains its identity through the whole cycle and that its trajectory involves a succession of continuous segments described by (4.1) that are interrupted by instantaneous frictionless jumps from the rear to the front. Notice that in this interpretation the blocks can change order and the condition $x_1 < x_2 < x_3$ is not always satisfied. For instance, when the blocks x_1 and x_2 collide at point B, the block x_1 disappears at the back (point B) and reappears at the front (point C) ahead of the block x_3. This jump mimics the frictionless part of the treadmilling cycle. It is clear that already in 2D formulation such jumps are not necessary because the reverse flow of actin can be modeled directly (see examples in the other chapters of this volume).

Consider now the case of N coupled blocks. Then, the force balance for the central blocks $j \in [2, N-1]$ reads

$$-l_b \xi \dot{x}_j - \chi_{j-1} + \chi_j - \eta \frac{\dot{x}_j - \dot{x}_{j-1}}{l_b} - \eta \frac{\dot{x}_j - \dot{x}_{j+1}}{l_b} = 0.$$

This system of equations can be written in the matrix form,

$$\mathbf{T}\dot{\mathbf{x}} = \mathbf{b}, \tag{4.4}$$

where we denoted by $\dot{\mathbf{x}}$ the unknown vector $\dot{x}_1, \ldots, \dot{x}_N$. The tri-diagonal matrix

$$\mathbf{T} = \begin{bmatrix} -(2+\frac{l_b^2}{l_0^2}) & 1 & 0 & 0 & 0 \\ 1 & -(2+\frac{l_b^2}{l_0^2}) & 1 & 0 & 0 \\ 0 & \ddots & \ddots & \ddots & 0 \\ 0 & 0 & 1 & -(2+\frac{l_b^2}{l_0^2}) & 1 \\ 0 & 0 & 0 & 1 & -(2+\frac{l_b^2}{l_0^2}) \end{bmatrix}$$

describes the viscous coupling and frictional interaction with the background while the vector

$$\mathbf{b} = \frac{l_b}{\xi l_0^2} \begin{bmatrix} -\chi_1 + \sigma_0 - \frac{\xi l_0^2}{l_b}\dot{x}_1 \\ \chi_1 - \chi_2 \\ \vdots \\ \\ \chi_{N-2} - \chi_{N-1} \\ \chi_{N-1} - \sigma_0 - \frac{\xi l_0^2}{l_b}\dot{x}_N \end{bmatrix}$$

with $\sigma_0 = -k(x_N - x_1 - L_0)/L_0$ carries the information about the active forcing, the mean field type elasticity and the boundary layer effects. To find the solution $\dot{\mathbf{x}}$, we need to invert the matrix $\mathbf{T}$ and then solve a system of two coupled linear equations $\dot{x}_1 = (\mathbf{R}\,\mathbf{b})_1$ and $\dot{x}_N = (\mathbf{R}\,\mathbf{b})_N$ where $\mathbf{R} = \mathbf{T}^{-1}$. The components of the matrix $\mathbf{R}$ can be found explicitly [98]

$$R_{i,j} = \frac{\cosh\left((N+1-j-i)\lambda\right) - \cosh\left((N+1-|j-i|)\lambda\right)}{2\sinh(\lambda)\sinh((N+1)\lambda)},$$

where $\lambda = \operatorname{arccosh}(1 + l_b^2/2l_0^2)$. Knowing the 'velocity field', we can now compute the steady state value of the length

$$L = L_0\left(1 - \frac{\sum_{j=1}^{N-1}\cosh(\lambda(j-N/2))\chi_j}{\sum_{j=1}^{N-1}\cosh(\lambda(j-N/2))k}\right).$$

From this formula we see again that a finite stiffness is necessary to prevent the collapse of the system under the action of contractile stresses: assuming for instance that $\chi_i = \bar{\chi}$ we obtain the low bound for the admissible elasticity modulus $k > \bar{\chi}$.

The steady velocity $V = (\dot{x}_N + \dot{x}_1)/2$ of the geometrical center of the system can be also computed explicitly

$$V = -\frac{l_b \sum_{j=1}^{N-1} \sinh(\lambda(j - N/2))\chi_j}{2\eta \sinh(\lambda N/2)}.$$

For N even, by denoting $M = N/2$, we can rewrite this expression in the form

$$V = -\frac{l_b \sum_{j=1}^{M-1} \sinh(j\lambda)(\chi_{M+j} - \chi_{M-j})}{2\eta \sinh(\lambda M)}$$

from where it is clear that (as in the case of three blocks) the symmetry of the vector χ with respect to the center must be broken for the system to be able to self-propel. An interesting mathematical problem associated with the absence of commutation between the zero viscosity limit and the continuum limit is discussed in [126].

4.2.2 Continuum Thermodynamics

Quite expectantly, our toy model of contraction-dominate crawling, has left us with many unanswered questions. For instance, it is not clear what is the microscopic nature of the active contraction forces χ_1 and χ_2 introduced ad hoc in the discrete model and how does the system creates and maintains the asymmetry $\chi_1 \neq \chi_2$. To answer these and other related questions we need to formulate a consistent thermo-mechanical continuum model that can be viewed as a limit of our discrete model but which goes much beyond it in detailing the physical mechanisms of both symmetry breaking and symmetry recovery.

To our advantage, such theory already exists [75, 82, 96] and the goal of this section will be to adapt it to our needs. It is known as the active gel theory and its main idea is the local orientation-induced tensorial coupling of chemistry and mechanics. Even though in a one dimensional setting the orientational order is trivial, this general framework will allow us to point out directly where the 'activity' assumption is embedded into the general continuum mechanical formulation. In contrast to previous expositions of the active gel theory where the main emphasis was on force balance, here we emphasize the energetic side of the chemo-mechanical coupling, see also [125].

Denote by $l_-(t)$ and $l_+(t)$ the moving rear and front boundaries of a one-dimensional segment occupied by a continuum body. We suppose that the system is driven externally, by applied forces, and internally, by chemical reactions. To describe the resulting motion we follow the standard approach of continuum mechanics [42]. First we introduce mass density $\rho(x, t)$ and velocity $v(x, t)$ satisfying the mass balance equation

$$\partial_t \rho + \partial_x(\rho v) = 0, \tag{4.5}$$

which was automatic in the discrete model. Since in this section the main focus is on contraction, we assume that there is no external mass flux (no growth)

$$\dot{m} = \rho_+[\dot{l}_+(t) - v(l_+(t), t)] = \rho_-[\dot{l}_-(t) - v(l_-(t), t)] = 0,$$

or

$$\dot{l}_\pm(t) = v(l_\pm(t), t).$$

We modify this assumption in Sects. 4.3 and 4.4 to account for active polymerization.

To write the momentum balance equation we introduce the stress $\sigma(x, t)$ and assume that the body is loaded by bulk forces $g(x, t)$ (friction forces in the discrete model). Then assuming that the inertial effects can be neglected we can write for the bulk points

$$\partial_x \sigma = g \tag{4.6}$$

which the analog of (4.1) in the discrete setting. We also assume that dead tractions $\sigma_0^\pm$ are applied at the moving boundaries $l_\pm$, so that $\sigma(l_\pm) = \sigma_0^\pm$. Notice that the 'volume preserving' global spring which was an essential feature of the discrete model can be also absorbed into $\sigma_0^\pm$ as will be made clear when we discuss physiologically meaningful boundary conditions in the next section.

Suppose that our continuum body is a mixture of active and passive components and that the mass fraction of the active component (a factor distinguishing between χ_1 and χ_2 in the discrete model) satisfies the balance equation

$$\rho\dot{\phi} = \partial_x J, \tag{4.7}$$

where J is the flux of the active component. The 'activity' of the active component has been so far fully implicit and the term itself will be justified only at the end of this section.

Next, we assume that there is a chemical reaction, responsible for contraction and implicit in the discrete setting, which proceeds with the rate ν per unit mass, so that

$$\rho(\partial_t \zeta + v\partial_x \zeta) = \nu, \tag{4.8}$$

where ζ is the reaction progress variable. For analytical simplicity we also postulate that our 'active' material is infinitely compressible (recall that connectors between the blocks in the discrete model did not contain regular elastic springs) and that the dynamics is isothermal. Then the free energy density can be written as $f = f(\phi, \zeta)$.

Four the four unknown functions $\phi(x, t)$ $\zeta(x, t)$, $\rho(x, t)$ and $v(x, t)$ we now have four equations (4.5)–(4.8), however, even if the functional dependence of the free energy density on its arguments is known, they still contain unidentified entities

σ, ν and J. To introduce constitutive relations linking these entities with our main unknown functions, we start with the expression for the global dissipation in the system $W - \dot{F} = R \geq 0$, where $F = \int_{l_-}^{l_+} \rho f dx$ is the total free energy of the system. If we introduce notation $[Q]_-^+ = Q^+ - Q^-$, we can write the power of external forces W in the form

$$W = -\int_{l_-}^{l_+} g v dx + [\sigma_0 \dot{l}]_-^+ = \int_{l_-}^{l_+} (-gv + \partial_x(\sigma v)) dx = \int_{l_-}^{l_+} \sigma \partial_x v dx.$$

Using mass balance equation we can also write

$$\dot{F} = \int_{l_-}^{l_+} (\partial_t \rho f + \rho \partial_t f) dx + [\rho f \dot{l}]_-^+ = \int_{l_-}^{l_+} \rho(\partial_t f + v \partial_x f) dx + \dot{m}[f]_-^+.$$

Since in this section we neglect active treadmilling $\dot{m} = 0$ and we obtain

$$\dot{F} = \int_{l_-}^{l_+} \rho \dot{f} dx = \int_{l_-}^{l_+} \rho(-A\dot{\zeta} + \mu \dot{\phi}) dx,$$

where $A(\phi, \zeta) = -\partial_\xi f$ is the affinity of the reaction and $\mu(\phi, \zeta) = \partial_\phi f$ is the chemical potential of the active component of the mixture. Assuming that there is no external flux of the active component through the boundaries, we finally write the expression for dissipation R in the form

$$R = \int_{l_-}^{l_+} (\sigma \partial_x v + \nu A + J \partial_x \mu) dx. \tag{4.9}$$

The three terms under the integral in (4.9) can be interpreted as products of the thermodynamic fluxes $\sigma, \rho\dot{\zeta}, J$ and the conjugate thermodynamic forces $\partial_x v, A, \partial_x \mu$. In the absence of microscopic models, we make a simplifying assumption that fluxes and forces are related linearly but since the system is at a finite distance from equilibrium, we allow the coefficients in these relations may be state (ϕ, ζ, ρ, v) dependent.

To further simplify the model we assume that diffusion is decoupled from the other two non-equilibrium mechanisms and write

$$J = l_{33} \partial_x \mu. \tag{4.10}$$

If we now define the mass density of the active component as $c = \phi\rho$ (we use different types of letters, c and ρ, for physically similar quantities to stress their different roles in the theory), we obtain the advection diffusion equation

$$\partial_t c + \partial_x(cv) = \partial_x(l_{33} \partial_x \mu),$$

where $l_{33} \geq 0$ is a mobility per unit volume.

We further suppose that reaction and deformation are coupled (chemo-mechanical effect, introduced for passive systems in [51]) so that

$$\begin{aligned} \sigma &= l_{11}\partial_x v + l_{12}A \\ \nu &= -l_{12}\partial_x v + l_{22}A. \end{aligned} \tag{4.11}$$

Here $l_{11} = \eta \geq 0$ is the standard Newtonian viscosity and l_{22} is a linearized reaction rate. The simplest way to express the fact that the active component plays a role of a catalyst for the reaction is to assume that $l_{22} = bc$ where b is a constant. Similarly, we assume that the reaction-deformation coupling is amplified in the presence of the active component and write $l_{12} = ac$, where a is another constant.

The first consequence of (4.11) is the constitutive relation

$$\sigma = \eta\partial_x v + aAc, \tag{4.12}$$

where the second term in the right hand side represents the 'active' stress emerging from mechano-chemical coupling. We assume that $a > 0$ which ensures that the reaction induced stresses are contractile whenever $A > 0$. Notice that (4.12) is the continuum analog of the corresponding relation in the discrete model where we implicitly used the notation $\chi = aAc$ and assumed that the right hand side depends on location of the corresponding bond but not on time.

The second consequence of (4.11) is the mechanical feedback to kinetics

$$\partial_t \zeta + v\partial_x \zeta = \phi(bA - a\partial_x v). \tag{4.13}$$

In the cell motility context, Eq. (4.13) describes spatial and temporal inhomogeneity of ATP hydrolysis supporting self-propulsion; observe that the reaction stops completely in the absence of 'active' component ($\phi = 0$).

To close the system we need to specify the expression for the free energy $f(\phi, \zeta)$. First of all we assume that the mixture is dilute and write

$$f = f_0(\zeta) + k_B T\phi \log \phi,$$

where k_B is the Boltzmann constant. Therefore $\mu = \mu_0 + k_B T \log \phi$ and $\partial_x \mu = k_B T\,(\partial_x c/c - \partial_x \rho/\rho)$. To recover a standard diffusion equation we need to make an additional assumption that the variation of the total density is small compared to the variation of the density of motors $\partial_x c/c \gg \partial_x \rho/\rho$. Then we can write $D = \varsigma k_B T$, where $\varsigma = l_{33}/c$ is the mobility per motor. To remain in the framework of Onsager theory of diffusion we need to assume that $c \sim \bar{c}$ and $l_{33} = l_{33}(\bar{c})$; this approximation clearly fails near the singularities of c where the model needs to be appropriately modified. Under these assumption we obtain that the density of the active component $c(x, t)$ satisfies the standard advection diffusion equation

$$\partial_t c + \partial_x(cv) - D\partial_{xx} c = 0. \tag{4.14}$$

To view this model from a slightly broader angle, consider a simple mixture model with two species representing attached and detached motors. The attached motors are advected with the velocity of actin filaments and can detach. The detached motors are freely diffusing, and can also attach. Suppose also that the attachment-detachment process can be described by a first order kinetic equation. Then the system of equations governing the evolution of the densities of attached c and detached c_d motors can be written as:

$$\begin{aligned}\partial_t c + \partial_x(cv) &= k_{\text{on}} c_d - k_{\text{off}} c \\ \partial_t c_d - \tilde{D}\partial_{xx} c_d &= k_{\text{off}} c - k_{\text{on}} c_d,\end{aligned}$$

where k_{on} and k_{off} are the chemical rates of attachment and detachment and $\tilde{D}$ is the diffusion coefficient of detached motors in the cytosol. Now suppose that the attachment-detachment process is chemically equilibrated and hence $c/c_d = K$, where $K = k_{\text{on}}/k_{\text{off}}$ is the reaction constant. Then for the attached motors performing contraction we obtain

$$((K+1)/K)\partial_t c + \partial_x(cv) - (\tilde{D}/K)\partial_{xx} c = 0.$$

Equation (4.14) is obtained in the limit $K \to \infty$ (fast attachment) and $\tilde{D}/K \to D$ (fast diffusion).

We now turn our attention to the dependence of the free energy on the reaction progress variable ζ. A standard assumption for a closed system would be that $f_0(\zeta)$ behaves quadratically around a minimum $\zeta = \zeta_0$ where $A = 0$. In this case ζ_0 represents equilibrium reaction progress. Instead, to emphasize the open nature of the system, we assume that

$$f_0(\zeta) = -A_0\zeta, \tag{4.15}$$

where $A_0 > 0$ is a prescribed constant measure of non-equilibrium. The seemingly innocent assumption (4.15) constitutes the main aspect of 'activity' in the model of active gel because all other constitutive elements of the model are conventional and passive [125].

The fact that the 'distance' from the equilibrium is independent of the reaction progress implies that there exists an exterior out of equilibrium chemostat. The 'bottomless' decrease of the free energy reflects the capability of the chemostat to continuously rebuild the non-equilibrium state. The energetic cost of such rebuilding must be compensated externally and the corresponding power delivered by the chemostat can be written as

$$\begin{aligned}-\dot{F} &= \int_{l_-}^{l_+} (\rho\dot{\zeta}A_0 + J\partial_x\mu)dx \qquad (4.16)\\ &= \int_{l_-}^{l_+} \left[gv + \eta(\partial_x v)^2 + bA_0^2\rho + D(k_{\text{B}}T/\bar{c})(\partial_x c)^2\right]dx \geq 0.\end{aligned}$$

This expression is quite natural: the first term in the right hand side describe the work against the applied force, while the other three terms characterize dissipation due to viscosity, reaction and diffusion. Equation (4.16) allows one to assess the efficiency of the underling active mechanism, see [125] for more detail.

The transparency of this model which becomes apparent in the next sections is due to the splitting of the main problem into several nested sub-problems. The main sub-problem is mechanical, providing a closed system of equation for v, σ and ρ. It includes the momentum balance equation (4.6), the constitutive equation (4.12) and the advection-diffusion equation (4.14) that are coupled through the velocity field. The second sub-problem concerns the transport of mass and the corresponding balance equation (4.5) can be solved once the velocity field v is known. The solution of this sub-problem provides ρ. The transport problem decouples from the mechanical problem because of the assumption of infinite compressibility indicating that the thermodynamical stress is equal to zero and the density variations do not affect the momentum balance. The last sub-problem concerns the reaction progress Eq. (4.13) that requires for its solution the knowledge of the velocity field v, the mass density ρ and the active component density c and which provides us with the field ζ. The kinetic equation decouples from the force balance and the mass transport problems because of the assumption that the free energy f does not depend on ρ and depends on ϕ and ζ only additively. Both of these assumptions are made to ensure analytic simplicity and can be easily dropped in numerical experiments.

4.2.3 Specialization of the Model

We now accommodate our general theory for the modeling of the lamellipodium viewed as a one dimensional continuum layer in frictional contact with a rigid background. Assuming that in (4.6) the friction is viscous $g(x,t) = \xi v(x,t)$ we write the force balance in the form

$$\partial_x \sigma = \xi v. \tag{4.17}$$

Equation (4.17) is the continuous analog of the system (4.4) in the discrete problem and similar to the discrete model, we denoted by ξ the coefficient of viscous friction [48, 61, 75, 86, 131, 141]. A microscopic justification of the idea that the time-averaged shear stress generated by constantly engaging and disengaging focal adhesions is proportional to the velocity of the retrograde flow can be found in [149]. There is evidence (both experimental [22, 53, 54, 102, 136] and theoretical [44, 99]) that this assumption describes the behavior of focal adhesions accurately only when the retrograde flow is sufficiently slow. The behavior of adhesion strength in the broader range of velocities is biphasic and since we neglect this effect, we potentially misrepresent sufficiently fast dynamics.

Following (4.12), see also [22, 67, 75, 83], we describe the constitutive behavior of the gel in the form

$$\sigma = \eta \partial_x v + \chi c, \tag{4.18}$$

where η is the bulk viscosity and $\chi = aA_0 > 0$ is a constant representing contractile pre-stress per unit motor mass. The constitutive relation (4.18) generalizes the parallel bundling of dashpots and contractile units in the discrete model. The important new element is that now the strength of the contractile elements is an unknown function which may vary in both space and time (in the discrete model the dependence of c on x was fixed). We assume that the function $c(x,t)$ satisfies the convection-diffusion equation (4.14). Behind this assumption is the idea that myosin motors, actively cross-linking the actin network, are advected by the network flow and can also diffuse due to thermal fluctuations [13, 22, 61, 131, 166].

To account for cortex/membrane elasticity and other means of volume control in a moving cell we further assume that, as in the discrete model, the boundaries of our moving active segment are linked through a linear spring [12, 49, 93, 124]. This assumption affects the values of the stress on the free boundaries $l_-(t)$ and $l_+(t)$:

$$\sigma_0^{\pm} = -k(L(t) - L_0)/L_0,$$

where $L(t) = l_+(t) - l_-(t)$ is the length of the moving segment, k is the effective elastic stiffness and L_0 is the reference length of the spring.

As in the general theory we assume that our self-propelling segment is isolated in the sense that $\dot{m} = 0$ and therefore the free boundaries move with the internal flow $\dot{l}_{\pm} = v(l_{\pm})$. We imply here that the addition and deletion of F-actin particles inserted at the front and taken away at the rear does not contribute to fronts propulsion. We also impose a zero flux condition for the active component $\partial_x c(l_{\pm}(t), t) = 0$ ensuring that the average concentration of motors

$$c_0 = \frac{1}{L_0}\int_{l_-(t)}^{l_+(t)} c(x,t)dx \tag{4.19}$$

is preserved. To complete the setting of the ensuing (statically determinate) mechanical problem we impose the initial conditions $l_{\pm}(0) = l_{\pm}^0$ and $c(x,0) = c^0(x)$.

If we now normalize length by L_0, time by L_0^2/D, stress by k, concentration by c_0 and density by M/L_0, we can rewrite the main system of equations (4.17), (4.18), (4.14) in dimensionless form (without changing the notations)

$$\begin{aligned} -\mathscr{Z}\partial_{xx}\sigma + \sigma &= \mathscr{P}c, \\ \partial_t c + \mathscr{K}\partial_x(c\partial_x\sigma) &= \partial_{xx}c. \end{aligned} \tag{4.20}$$

Here we introduced three main dimensionless constants of the problem: $\mathscr{Z} = \eta/(\xi L_0^2)$—the scale of viscous interaction; $\mathscr{K} = k/(\xi D)$—the non-dimensional measure of diffusion and finally $\mathscr{P} = c_0\chi/k$—the scale of contractility. In (4.20) one immediately sees the structure of the Keller–Segel system from the theory of chemotaxis, e.g. [112]. The role of the distributed chemical attractant is played by the stress field σ whose gradient is the driving force affecting the 'colony' of myosin motors. Therefore in this model [124, 125] the spontaneous localization, which is a typical feature of chemotaxis, is driven by mechanical rather than chemical gradients.

We refer to the mechanism of generating and sustaining mechanical inhomogeneities described by system (4.20) as autotaxis [123]. In physical terms it can be characterized as follows. Suppose that the motor proteins (our active component) with sufficient contractility induce internal stress which can overcome the hydrodynamic resistance and induce flow. The flow produces a drift of motors in the direction of the regions where they concentrate and such autocatalytic amplification is the mechanism of the positive feedback in our model. The ensuing runaway is countered by diffusion of active component which penalizes creation of concentration gradients and thus plays the role of a negative feedback. When a critical contractility of active component is reached, the homogeneous distribution of motors becomes unstable. The contraction asymmetry then induces a flow of actin filaments towards the trailing edge thus producing frictional forces which propel the cell forward. The eventual build up of a balance between drift and diffusion leads to the formation of a pattern. As we show below, among various admissible patterns, whose number increases with contractility, the stable ones localize motors at the trailing edge as observed in experiments.

The main mathematical difference between ours and the standard chemotaxis problem is that we have free boundaries. Using dimensionless variables we can rewrite the boundary conditions in the form

$$\dot{l}_{\pm}(t) = \mathscr{K}\,\partial_x \sigma(l_{\pm}(t), t), \tag{4.21}$$

$$\sigma(l_{\pm}(t), t) = -(L(t) - 1), \tag{4.22}$$

$$\partial_x c(l_{\pm}(t), t) = 0 \tag{4.23}$$

while the integral constraint (4.19) reduces to $\int_{l_-}^{l_+} c(x,t)dx = 1$.

4.2.4 Non-Local Reformulation

Since the first of the equations (4.20) is linear, it can be solved explicitly for σ

$$\sigma(x,t) = -\frac{(L-1)\cosh[(G-x)/\sqrt{\mathscr{Z}}]}{\cosh[L/(2\sqrt{\mathscr{Z}})]} + \frac{\mathscr{P}}{\sqrt{\mathscr{Z}}}\int_{l_-}^{l_+} \Psi(x,y)c(y)dy, \tag{4.24}$$

where

$$\Psi(x,y) = \frac{\sinh[(l_+ - x)/\sqrt{\mathscr{Z}}]\sinh[(y-l_-)/\sqrt{\mathscr{Z}}]}{\sinh(L/\sqrt{\mathscr{Z}})} - H(y-x)\sinh[(y-x)/\sqrt{\mathscr{Z}}].$$

We introduced the notations: $H(x)$—the Heaviside function and $G(t) = [l_-(t) + l_+(t)]/2$ is the position of the geometric center of the moving fragment. By eliminating σ from $(4.20)_2$ we obtain a single non-local partial differential equation with quadratic nonlinearity for $c(x,t)$

$$\partial_t c(x,t) - \mathscr{K}(L-1)\partial_x[\theta(x)c(x,t)] + \frac{\mathscr{P}\mathscr{K}}{\sqrt{\mathscr{Z}}}\partial_x\Big(\int_{l_-}^{l_+}\varphi(x,y)c(y,t)c(x,t)dy\Big) = \partial_{xx}c(x,t), \tag{4.25}$$

where the auxiliary velocity field

$$\theta(x) = \frac{\sinh[(x-G)/\sqrt{\mathscr{Z}}]}{\cosh[L/(2\sqrt{\mathscr{Z}})]}$$

describes advective flow induced by the elastic coupling between the rear and the front of the active segment. The feedback behind contraction-driven motility is contained in the kernel

$$\varphi(x,y) = -\frac{\cosh[(l_+-x)/\sqrt{\mathscr{Z}}]\sinh[(y-l_-)/\sqrt{\mathscr{Z}}]}{\sinh(L/\sqrt{\mathscr{Z}})} + H(y-x)\cosh[(y-x)/\sqrt{\mathscr{Z}}],$$

which is due to viscosity-induced interactions in the system and the effect of the boundaries. Notice that this kernel has the action/reaction symmetry $\varphi(x,y) = -\varphi(l_+ + l_- - x, l_+ + l_- - y)$ which is a fundamental constraint imposed by the balance of momentum [79, 80, 154]. An interesting zero viscosity limit of the obtained system of equations leading to singular solutions is discussed in [126].

Using the boundary conditions (4.21) we find from (4.24) an explicit formula for the (time dependent) velocity of the center of our active segment

$$\dot{G} = \frac{\mathscr{K}\mathscr{P}}{2\mathscr{Z}}\int_{l_-}^{l_+}\frac{\sinh\left(\frac{G-x}{\sqrt{\mathscr{Z}}}\right)}{\sinh\left(\frac{L}{2\sqrt{\mathscr{Z}}}\right)}c(x,t)dx, \tag{4.26}$$

from which we infer that the maximal velocity of the self propelling segment is equal to $\mathscr{K}\mathscr{P}/(2\mathscr{Z})$. Similarly we obtain an equation for the evolving length of the segment

$$\dot{L} = -2\frac{\mathscr{K}}{\sqrt{\mathscr{Z}}}(L-1)\tanh\left(\frac{L}{2\sqrt{\mathscr{Z}}}\right) - \frac{\mathscr{K}\mathscr{P}}{\mathscr{Z}}\int_{l_-}^{l_+}\frac{\cosh\left(\frac{G-x}{\sqrt{\mathscr{Z}}}\right)}{\cosh\left(\frac{L}{2\sqrt{\mathscr{Z}}}\right)}c(x,t)dx. \tag{4.27}$$

Notice that in (4.26) only the odd component of the function $c(x,t)$ [with respect to the moving center $G(t)$] contributes to the integral while in (4.27) only the even component matters. In particular, if the concentration of motors is an even function of x then $\dot{G} = 0$ and the segment does not move as a whole. This statement is a direct analog of Purcell's theorem [119] for a crawling body.

Given our interest in the steady modes of cell motility, which are typical for keratocytes [13], we need to study the traveling wave (TW) solutions of the main system (4.20). To find such solutions we assume that the front and the rear of the segment travel with the same speed $\dot{l}_\pm(t) \equiv V$, ensuring the constancy of the length $L(t) \equiv L$, and that both the stress and the myosin concentration depend exclusively

on the appropriately chosen co-moving coordinate $u = (x - x_0 - Vt)/L_0 \in [-1/2, 1/2]$. Using this ansatz we find that Eq. (4.20)$_2$ can be solved explicitly

$$c(u) = \frac{\exp[s(u) - VLu]}{L\int_{-1/2}^{1/2} \exp[s(u) - VLu]du}. \tag{4.28}$$

Here for convenience we introduced a new stress variable $s(u) = \mathscr{K}[\sigma(u) + (L-1)]$ which represents the inhomogeneous contribution to internal stress field due to active pre-stress. The system (4.20) reduces to the single nonlocal equation

$$-\frac{\mathscr{Z}}{L^2}s''(u) + s(u) - \mathscr{K}(L-1) = \mathscr{K}\mathscr{P}\frac{\exp[s(u) - LVu]}{L\int_{-1/2}^{1/2} \exp[s(u) - VLu]du}, \tag{4.29}$$

supplemented by the boundary conditions

$$s(\pm 1/2) = 0 \quad \text{and} \quad s'(\pm 1/2) = LV. \tag{4.30}$$

The two 'additional' boundary conditions in (4.30) allow one to determine parameters V and L along with the function $s(u)$. After the problem (4.29), (4.30) is solved, the motor concentration profile can be found explicitly by using Eq. (4.28).

4.2.5 Static Solutions

Initiation of motility is associated with a symmetry breaking instability of a static (non-motile) solution. To identify non-motile configurations we need to find solutions of (4.29) with $V = 0$. Notice that these solutions may still describe the states with nontrivial active internal rearrangements of both actin and myosin [22].

If $V = 0$, Eq. (4.29) simplifies considerably

$$-\frac{\mathscr{Z}}{L^2}s'' + s - \mathscr{K}(L-1) = \mathscr{K}\mathscr{P}\frac{\exp(s)}{L\int_{-1/2}^{1/2} \exp(s(u))du}. \tag{4.31}$$

The nonlocal Eq. (4.31) was studied extensively in many domains of science from chemotaxis [140] to turbulence [27] and gauge theory [148]. In our case, this equation where parameter L remains unknown, has to be solved with three boundary conditions $s'(-1/2) = s(\pm 1/2) = 0$ because the forth boundary condition $s'(1) = 0$ is satisfied automatically.

We begin with the study of the regular solutions of (4.31). Instead of $\mathscr{K}$ and $\mathscr{P}$, it will be convenient to use another set of parameters $A := \mathscr{K}(L-1) \leq 0$ and $B := \mathscr{K}\mathscr{P}/(L\int_{-1/2}^{1/2} \exp[s(u)]du) \geq 0$. In terms of parameters (A, B) the problem (4.31) reads

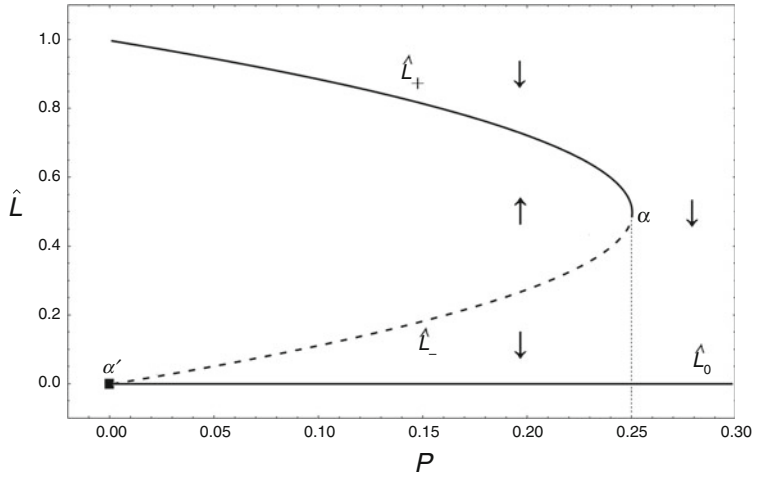

Fig. 4.3 Three families of trivial static solutions $\hat{L}_+, \hat{L}_-$ and $\hat{L}_0$ parameterized by $\mathscr{P}$. *Solid lines* show stable branches while *dotted lines* correspond to unstable branches. *Arrows* depict the basin of attraction of each branch

$$-\frac{\mathscr{Z}}{L^2}s'' + s - A = B\exp(s) \quad \text{with} \quad s'(-1/2) = s(\pm 1/2) = 0. \tag{4.32}$$

A trivial homogeneous solution of this problem $s(u) = 0$ exists when $A + B = 0$ which is equivalent in the $(\mathscr{P}, \mathscr{K})$ parametrization to $L = \hat{L}_\pm$ with,

$$\hat{L}_\pm = (1 \pm \sqrt{1 - 4\mathscr{P}})/2. \tag{4.33}$$

The sub-branches with longer and shorter lengths $\hat{L}_+(\mathscr{P})$ and $\hat{L}_-(\mathscr{P})$, respectively, that meet at point α where $\hat{L}_-(\mathscr{P}) = \hat{L}_+(\mathscr{P})$ are illustrated in Fig. 4.3.

To obtain nontrivial static solutions we multiply (4.32) by s', integrate and use the boundary conditions to obtain the 'energy integral' $s'^2 = W(s)$, where

$$W(s) = \frac{L^2}{\mathscr{Z}}(s^2 - 2As - 2B\,[\exp(s) - 1]).$$

The general solution of this equation can be expressed as a quadrature,

$$u = \pm \int^{s(u)} W^{-1/2}(r)dr.$$

A detailed analysis of these solutions can be found in [126].

In addition to regular solutions described above Eq. (4.31) has measure-valued solutions corresponding to collapsed cells with length $\hat{L}_0 = 0$. First of all, as we see in Fig. 4.3, $\hat{L}_-(\mathscr{P}) \to 0$ when $\mathscr{P} \to 0$ (point α') and therefore the limiting

distribution of motors is concentrated on an infinitely small domain. To characterize the asymptotic structure of such singular solutions we suppose that $L \gg 1$ and that the maximum of s is of order L. Then, by ignoring higher order terms, we deduce from (4.31) a simplified boundary value problem

$$-s'' \approx \mathscr{K}\mathscr{P}L/(\mathscr{Z}\int_{-1/2}^{1/2}[1+s(u)]du) \quad \text{with} \quad s'(-1/2) = s(\pm 1/2) = 0. \tag{4.34}$$

Then $s(u) \approx \mathscr{K}\mathscr{P}L(1/2+u)(1/2-u)/(2\mathscr{Z})$ and the remaining boundary condition $s'(-1/2) = 0$ is automatically satisfied in the limit $L \to 0$. We can then conclude that the singular solutions are of the form $s(x) = \lim_{L\to 0} Lf(x/L)$, where $f(u) = \mathscr{K}\mathscr{P}(1/2+u)(1/2-u)/(2\mathscr{Z})$. Singular solutions of this type can be useful in the description of cell splitting in a cortical geometry [156]; they are also known in other fields where stationary states are described by Eq. (4.31) [27, 36, 56, 108]. The presence of such solutions is a sign that in a properly augmented theory, accounting for the vanishing length, one can expect localization with active contraction balanced by a regularization mechanism, say active treadmilling [124] . Our numerical solutions of a non-steady problem, which are naturally regularized because of the finite mesh size, show that the almost singular solutions of the type described above serve as attractors for initial data with $L < \hat{L}_-$ when $\mathscr{P} < 1/4$. Moreover, numerical experiments suggest that they are the only attractors for $\mathscr{P} > 1/4$. This means that even in the presence of a cortex-type spring, an active segment fragment necessarily collapses after the contractility parameter reaches the threshold $\mathscr{P}_{\max} = 1/4$.

4.2.6 Linear Stability

We first show that motile branches with $V \neq 0$ can bifurcate only from trivial static solutions with $s(u) = 0$, $V = 0$ and $L = \hat{L}_\pm$. If $V \neq 0$ we can multiply (4.29) by $s' - VL$, to find that

$$\exp(LV/2) - \exp(-LV/2) = LV\int_{-1/2}^{1/2}\exp[s(u) - VLu]du. \tag{4.35}$$

From (4.35), in the limit $V \to 0$ we obtain that $\int_{-1/2}^{1/2}\exp(s(u))du = 1$. Since static solutions $s(u)$ must be necessarily sign definite [126] the limiting static solution can be only trivial $s(u) = 0$. As we have seen in Fig. 4.3, there are two non-singular families of trivial solutions: one with longer ($\hat{L}_+$ family) and the other with shorter ($\hat{L}_-$ family) lengths.

To find the bifurcation points along the trivial branch $[s = 0, V = 0, L = \hat{L}_\pm(\mathscr{P})]$, we introduce infinitesimal perturbations $\delta s(u)$, δV, δL and linearize (4.29) together with boundary conditions (4.30). We obtain the boundary value problem

$$\delta s'' - \omega^2 \delta s = \frac{\mathscr{Z}\omega^2 - \hat{L}^2}{\hat{L}^2(\hat{L}-1)} \left(\mathscr{Z} \frac{2\hat{L}-1}{\hat{L}} \omega^2 \delta L + \hat{L}^3(\hat{L}-1) u \delta V \right), \tag{4.36}$$

$$\delta s(\pm 1/2) = 0, \quad \delta s'(\pm 1/2) = \hat{L}\delta V, \tag{4.37}$$

where we introduced the notation $\omega^2 = (\hat{L}^2 - \mathscr{K}\mathscr{P}\hat{L})/\mathscr{Z}$. Since $\omega = 0$ at the trivial branch $\delta s = \delta V = \delta L = 0$, we can assume that $\omega \neq 0$. The general solution of the problem (4.36), (4.37) can be written explicitly

$$\begin{aligned} \delta s(u) = {} & C_1 \sinh(-\omega u) + C_2 \cosh(-\omega u) \\ & - \frac{\mathscr{Z}\omega^2 - \hat{L}^2}{\omega^2 \hat{L}^2(\hat{L}-1)} \left(\mathscr{Z} \frac{2\hat{L}-1}{\hat{L}} \omega^2 \delta L + \hat{L}^3(\hat{L}-1) u \delta V \right). \end{aligned}$$

Using boundary conditions (4.37) we obtain a transcendental equation for ω

$$2\hat{L}[\cosh(\omega) - 1] - \mathscr{K}\mathscr{P}\omega \sinh(\omega) = 0. \tag{4.38}$$

The detailed analysis of this equation is presented in [126]. Here we only show the locus of bifurcation points in the $(\mathscr{K}, \mathscr{P})$ plane (Fig. 4.4). For motile solutions we use notations D_i and for nontrivial static solutions—notations S_i where $i = 1, 2, \ldots$ In Fig. 4.4 the lines marked by $+$ and $-$ correspond to bifurcations originating on the trivial sub-branches $\hat{L}_+$ and $\hat{L}_-$, respectively.

If parameter $\mathscr{P}$ is held constant while $\mathscr{K}$ is changing each family D_i and S_i is represented by two points. For solutions bifurcating from the trivial branch $\hat{L}_+$, we have bifurcations at $\mathscr{K}_+ = (\hat{L}_+^2 - \mathscr{Z}\omega^2)/(\mathscr{P}\hat{L}_+)$, which gives points $D_1^+, S_1^+, D_2^+, S_2^+, \ldots$ and for the branch $\hat{L}_-$, bifurcations take place at $\mathscr{K}_- = (\hat{L}_-^2 - \mathscr{Z}\omega^2)/(\mathscr{P}\hat{L}_-)$ which gives points $D_1^-, S_1^-, D_2^-, S_2^-, \ldots$. Notice that the total number of bifurcation points increases to infinity as $\mathscr{K} \to \infty$.

Now consider the case when $\mathscr{K} = \text{const}$ and $\mathscr{P}$ is varied. A line $\mathscr{K} = \text{const}$ in the $(\mathscr{K}, \mathscr{P})$ plane cuts again each curve D_i and S_i in two points which we denote $D_1^*, S_1^*, \ldots$ (solutions with longer lengths) and $D_1^{**}, S_1^{**}, \ldots$ (solutions with shorter lengths), see Figs. 4.3 and 4.4. In most cases one of these two points is a bifurcation originating from the $\hat{L}_-$ trivial solution while the other is from the $\hat{L}_+$ trivial solution. However, as we show in the inset in Fig. 4.4 the two points may also bifurcate from the same branch $\hat{L}_+$. Such bifurcations are of particular interest because they describe both motility initiation and motility arrest.

After bifurcation points are known one can use the Lyapunov–Schmidt reduction technique to identify the nature of the corresponding bifurcations [9, 78, 106]. The analysis presented in [126] shows that the bifurcations from the trivial to the nontrivial static branch are always transcritical. The bifurcations to motile branches can be either subcritical or supercritical. In particular, at a given $\mathscr{K}$ the bifurcation from a static homogeneous solution with longer length is always supercritical while the bifurcation from a static homogeneous solution with smaller length can be either subcritical or supercritical depending on the value of $\mathscr{K}$, see [126].

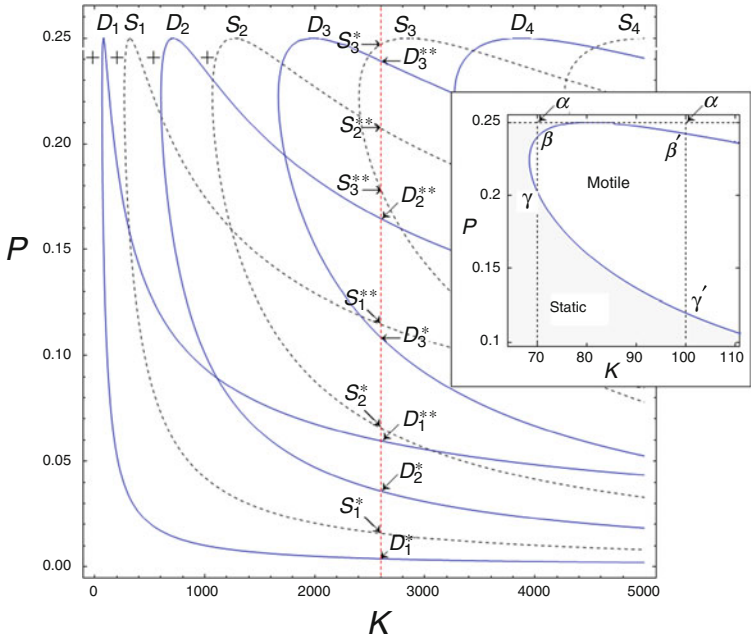

Fig. 4.4 Locus of the bifurcation points in the $(\mathscr{K}, \mathscr{P})$ plane for $\mathscr{Z} = 1$. *Inset* shows a zoom on the D_1 branch around the turning point at $\mathscr{P} = 1/4$ where $\hat{L}_-$ and $\hat{L}_-$ branches meet. The detailed bifurcation diagrams for $\mathscr{P} = 0.245$ and $\mathscr{K} = 70$ and 100 are shown in Figs. 4.5 and 4.6 from where the meaning of labels β, γ, β' γ' becomes clear. The bifurcation points related to the cut $\mathscr{K} = 2600$ (*red dashed line*) in the $(\mathscr{P}, L)$ space are shown in Fig. 4.3

4.2.7 Motile Solutions

To illustrate different types of nontrivial solutions of bifurcations we used the nonlinear continuation methods to solve the boundary value problem (4.29)–(4.30) numerically for successive values of parameters $\mathscr{K}$ and $\mathscr{P}$ (tracking algorithm, see [45]). In Fig. 4.5a we show the continuation in $\mathscr{K}$ for both static and motile configurations at fixed $\mathscr{P}$; the corresponding profiles of motor concentration, stress and velocity are shown in Fig. 4.5b. One can see that each pitchfork (for motile branches) and each transcritical (for static branches) bifurcation points gives rise to two nontrivial solutions. For instance, along the static branch $\hat{L}_+$, the bifurcation point D_1^+ is associated with two motile supercritical branches whereas the point S_1^+ is associated with two transcritical static branches. Each pair of motile solutions is symmetric with two opposite polarizations corresponding to two different signs of the velocity. Along the first motile branch originating at D_1^+, the myosin motors concentrate at the trailing edge. For the second motile branch originating at D_2^+, there is an additional peak in the concentration profile, see Fig. 4.5b. In contrast, the static bifurcation point S_1^+ gives rise to two symmetric configurations with different

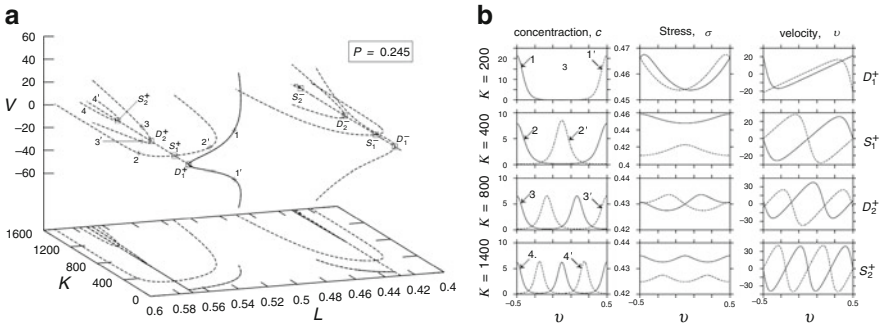

Fig. 4.5 (**a**) Bifurcation diagram with $\mathscr{K}$ as a parameter showing nontrivial solutions branching from families of homogeneous static solutions $\hat{L}_+$ and $\hat{L}_-$. The value $\mathscr{P} = 0.245$ and $\mathscr{Z} = 1$ are fixed. *Solid lines* show stable motile branches while all the *dotted lines* correspond to unstable solutions. The internal configurations corresponding to branches indicated by numbers $(1, 1', 2, 2'$,etc) are shown in (**b**). The projection of the bifurcation diagram on the $(\mathscr{K}, L)$ plane is also shown below. (**b**) Internal profiles associated with successive bifurcated solutions shown in (**a**) for $\mathscr{P} = 0.245$ and $\mathscr{Z} = 1$. Our notation (1,3) correspond to asymmetric motile branches while (2,4) describe symmetric static branches

lengths and with myosin motors concentrated either in the middle of the cell or near the boundaries, see Fig. 4.5b. As one would expect, the higher order static and motile bifurcation points produce solutions with more complex internal patterns. For the branches bifurcating from the trivial configurations belonging to $\hat{L}_-$ family, the picture is similar, see Fig. 4.5a.

In Fig. 4.6, we show in more detail the nontrivial solutions originating from the motile bifurcation points D_1 at two values of parameter $\mathscr{K}$ which correspond to two sections $\alpha\beta$ and $\alpha\beta'$ shown in Fig. 4.4 (insert). Notice that a single solution connects the bifurcation points D_1^* (suprecritical) and D_1^{**} (sub- or super-critical) which may belong either to one family $\hat{L}_+$ ($\alpha\beta$ where D_1^* is the same as D_1^+ and D_1^{**} is the same is D_1^+) or to two different families $\hat{L}_+$ and $\hat{L}_-$ ($\alpha\beta'$ where D_1^* is the same as D_1^+ and D_1^{**} is the same as D_1^-). In the former case, the nontrivial motile branch has a turning point at a finite value of $\mathscr{P} < 1/4$ giving rise to a re-entrant behavior. Similar behavior was also observed in some other models of cell motility, e.g. [55, 80, 153].

As illustrated in Fig. 4.6 and shown more clearly in a phase diagram in Fig. 4.7a, in the re-entrant regime (sufficiently low $\mathscr{K}$), the increase of the average concentration of myosin (increase of $\mathscr{P}$ at fixed $\mathscr{K}$) first polarizes the cell and initiates motility, but then, if the contractility is increased further, the cell may becomes symmetric again by re-stabilizing in another static homogeneous configuration (see Fig. 4.6, $\mathscr{K} = 70$). We reiterate that re-symmetrization and arrest prior to division (known also as 'mitotic cell rounding') is a common feature of almost all animal cells [84, 85, 145]. In this respect, it is interesting that if contractility ($\mathscr{P}$) is increased further, the cell collapses to a point because our effective 'size preserving spring' cannot support the contraction any more. Following [156], we can associate

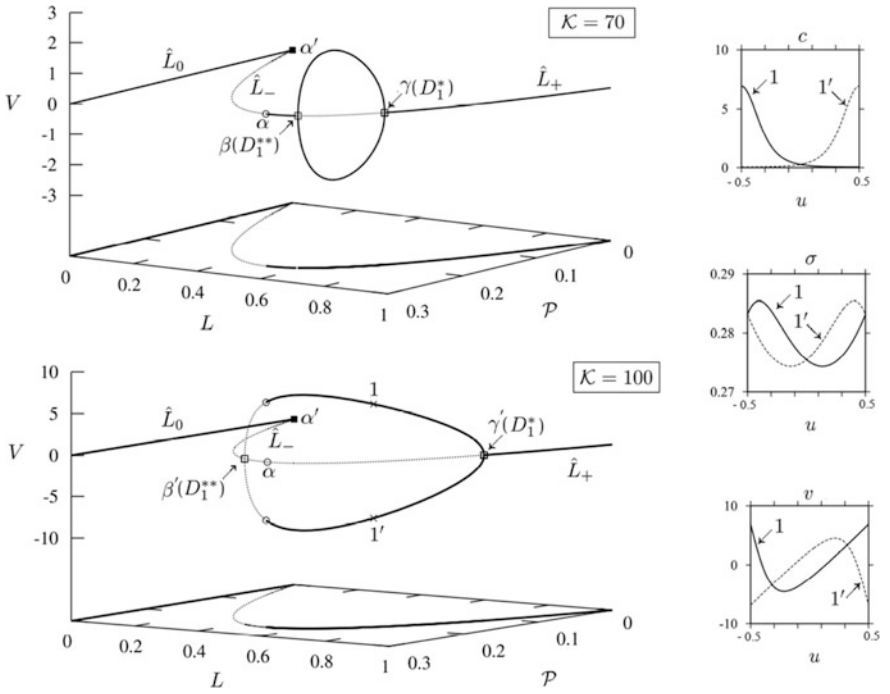

Fig. 4.6 Bifurcation diagrams along parameter $\mathscr{P}$ showing motile branches connecting points D_1^* and D_1^{**}. Corresponding bifurcation points are shown in *insert* in Fig. 4.4. *Solid lines* show stable motile branches while all the *dotted lines* correspond to unstable solutions. The projection of the bifurcation diagram on the $(\mathscr{P}, L)$ plane is also shown. Parameter $\mathscr{K}$ is fixed in each graph to $\mathscr{K} = 70$ and $\mathscr{K} = 100$. Internal profiles on the two symmetric motile branches are also shown for $\mathscr{K} = 100$. Parameter $\mathscr{Z} = 1$

such collapse with cell division. We can then argue that our deliberately minimal model succeeds in reproducing a rather general pattern of cell behavior by showing that symmetrization (stabilization) in space immediately precedes the division.

While the physical meaning of the non-dimensional parameter $\mathscr{P}$ in this discussion is rather clear (contractility measure), the significance of varying $\mathscr{K}$ at fixed $\mathscr{Z}$ is less obvious because both of these parameters depend on frictional strength of the background. Adhesivity of the cell to the substrate is known to be a crucial parameter for motility initiation and arrest for various cell types [10, 91]. To explicitly expose the role of friction, it is instructive to interpret parameter $1/\mathscr{K}$ as a measure of adhesivity while keeping the ratio $\mathscr{Z}/\mathscr{K}$, which does not have any relation to friction, at a constant level.

The phase diagram in the $(\mathscr{P}, 1/\mathscr{K})$ plane at fixed $\mathscr{Z}/\mathscr{K}$ is shown in Fig. 4.7b. In this diagram a horizontal path extending from left to right describes a succession of states with fixed adhesivity and increasing contractility. One can see that at high adhesivity motility ceases to exist, moreover as contractility increases static solutions eventually collapse. If the adhesivity is below a certain threshold, the

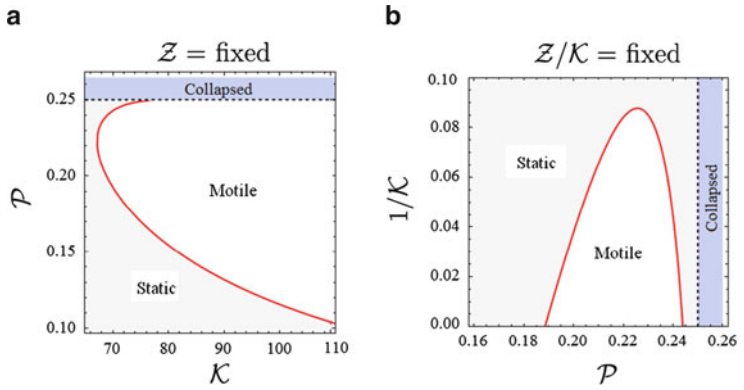

Fig. 4.7 (**a**) Phase diagram of the system (4.20) in the parameter plane $(\mathscr{K}, \mathscr{P})$ at fixed $\mathscr{Z} = 1$. (**b**) Phase diagram of the same system (4.20) in the parameter plane $(\mathscr{P}, 1/\mathscr{K})$ at fixed $\mathscr{Z}/\mathscr{K} = 0.015$. The *solid* (*red*) line indicates the motile bifurcation point (D_1^+ similar to Fig. 4.4), while the *black dashed lines* indicate the collapse threshold ($\mathscr{P}_{\max} = 1/4$)

contractility increase first causes polarization of a static configuration and motility initiation; further increase of contractility causes re-symmetrization, arrest and eventually collapse. An interesting regime corresponds to the very tip of the motile domain shown in Fig. 4.7b. Near this 'critical' point the motility can be sustained in a narrow 'homeostatic window' of parameters and can be easily arrested by either increase or decrease of contractility.

Very recently new experimental results elucidating motility initiation in fish keratocytes have appeared [14]. According to these experiments, at a fixed contractility level (fixed $\mathscr{P}$ in our model), the increase of surface adhesivity (increase of $1/\mathscr{K}$ in our model) promotes static configurations while lowering adhesivity initiates motility. As it follows from Fig. 4.7b, these observations are in agreement with our predictions. Our model also explains another observation made in [14] that at a fixed adhesivity, a blebbstatin (a contractility inhibitor) treatment promotes arrest of the cells while a calyculin A treatment (a contractility stimulator) initiates motility. The question whether a more substantial increase of contractility in experiment can lead to re-symmetrization and arrest remains open. It is promising in this respect that some cells are known to undergo static to motile transformation in response to a *decrease* in the level of contractility [68, 90]. The minimal model presented in [14] is exactly a 2D version of the one formulated in [122] and further developed in the present paper. While active protrusion and nonlinear regulation of adhesion were also accounted for in [14] to get a realistic cell shape, it is rather remarkable that the fundamental pattern of motility initiation (including its dependence on contractility and adhesivity) can be already captured within our much more transparent setting, see Fig. 4.7b and [126].

Among various branches of the TW solutions studied above only stable ones have physical sense. The stability was studied numerically in [123] and here we briefly summarize the results of the solution of the corresponding perturbed initial value problems.

The numerical experiments suggest that the trivial branch $\hat{L}_-$ is unstable together with all nontrivial non-singular static solutions. The singular static solutions from the $\hat{L}_0$ family appear to be locally stable. Instead, the dynamic solutions are all unstable except for the branches bifurcating from the points D_1^+ on the trivial branch $\hat{L}_+$. The trivial branch $\hat{L}_+$ branch is locally stable until the first (motile) bifurcation D_1^+. Both symmetric subbranches of D_1^+ (subfamilies 1 and $1'$ in Fig. 4.5a, b are stable and this justifies the above speculations about motility initiation and motility arrest. Moreover, we found that some unstable multi-peaked static and dynamic solutions are long living. This behavior, which was also observed in [22, 67, 80] in the problem with fixed boundaries, is reminiscent of the spinodal decomposition in a 1D Cahn–Hilliard model where the coarsening process gets critically slowed down near multiple saddle points [35].

4.2.8 *Passive Actin Treadmilling*

We recall that our assumption that the bulk stiffness of the cytoskeleton is equal to zero (infinite compressibility assumption [75, 131]) allowed us to uncouple the force balance problem from the mass transport problem. As we have seen in the previous section, by solving our Keller–Segel system we can obtain the velocity field and the concentration of motors. To recover the mass distribution of the cytoskeleton we need to solve a decoupled mass balance equation (4.5) with a kinematically prescribed velocity field and initial condition $\rho(x,0) = \rho_0(x)$. Knowing $v(x,t)$ also means that we know trajectories of the free boundaries $l_-(t)$ and $l_+(t)$ and since both edges move with the particles the total mass $M = \int_{l_-(t)}^{l_+(t)} \rho(x,t)dx$ is conserved.

In dimensionless variables the mass balance equation (4.5) can be written as

$$\partial_t \rho + \mathscr{K}\partial_x(\rho\partial_x\sigma) = 0 \tag{4.39}$$

and the total mass constraint takes the form $\int_{l_-(t)}^{l_+(t)} \rho(x,t)dx = 1$. Supposing that the velocity field $v(x,t) = \mathscr{K}\partial_x\sigma(x,t)$ is known, we solve (4.39) by the method of characteristics. Denote the trajectories of the mass particles by $x = x(\zeta,t)$, where $l_-(0) \le \zeta \le l_+(0)$ is the Lagrangian coordinate at $t = 0$, the characteristic curves can be found from the equations

$$\frac{dx(\zeta,s)}{ds} = v(x(\zeta,s),s). \tag{4.40}$$

Along these curves we must have

$$\frac{d\rho(x(\zeta,s),s)}{ds} = -\rho(x(\zeta,s),s)\partial_x v(x(\zeta,s),s).$$

Integration of this equation gives an explicit formula for the mass density

$$\rho(x(\zeta,t),t) = \rho_0(\zeta)\exp\left\{-\int_0^t \partial_x v(x(\zeta,s),s)ds\right\}. \tag{4.41}$$

For TW solutions of (4.20), the velocity field in (4.40) depends on the normalized co-moving variable u and the normalized Lagrangian variable $\hat{\zeta} = \zeta/L(0) - 1/2$, both in the interval $[-1/2, 1/2]$. Then $v = v(u)$ and Eq. (4.40) reduces to

$$\frac{du(\hat{\zeta},s)}{ds} = \frac{v(u(\hat{\zeta},s)) - V}{L}. \tag{4.42}$$

For instance, close to the bifurcation points, for the motile branches $D_m^{\pm}$ we need to solve the characteristic equation

$$\frac{du(\hat{\zeta},s)}{ds} = \varsigma\left\{-\frac{L^2}{\omega_c^3\cos(\omega_c/2)}\left[\omega_c\cos(\omega_c u(\hat{\zeta},s)) - 2\sin(\omega_c/2)\right] - 1\right\}, \tag{4.43}$$

where ω_c is the corresponding solution of Eq. (4.38). In Fig. 4.8, we show the sample solutions of (4.43) corresponding to homogeneous initial conditions $u(\hat{\zeta},0) = \hat{\zeta}$ and positive ς.

According to (4.42) the points of the body where $v = V$ are singular because the relative flow there is stagnated. If at such point the slope of the function $v(u)$ is negative we obtain a sink of particle trajectories $u = \gamma_+$ (i.e. an attractor for particles as $t \to \infty$) whereas if the slope of the function $v(u)$ is positive, the singular point $u = \gamma_-$ corresponds to a source of particle trajectories (an attractor as $t \to -\infty$). Then all mass points (corresponding to different values of $\hat{\zeta}$) come from

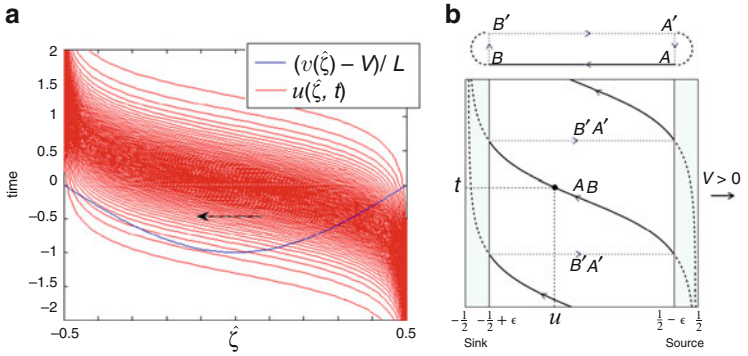

Fig. 4.8 (**a**) Trajectories of particles from a source to a sink for the first motile bifurcation point associated with positive velocity for initially homogeneously distributed set of particles. (**b**) Trajectory of an individual actin particle undergoing passive treadmilling for a typical solution on the D_1 motile branch with $V > 0$. *Shaded regions* are excluded domains of singular behavior

the sources where the characteristic curves accumulate at large negative times and disappear in the sinks where the characteristic curves accumulate at large positive time. An important feature of the flows described by (4.42) is that it takes an infinite time for a mass particle to reach a sink or to leave a source because $(v(u) - V)^{-1}$ is not integrable in the neighborhood of γ_- and γ_+. As a result the total mass flux is equal to zero

$$\dot{m} = \left(\int_{\gamma_-}^{\gamma_+} \frac{du}{v(u) - V} \right)^{-1} = 0.$$

To illustrate this point we recall that for the TW solutions the general formula (4.41) describing the mass distribution simplifies

$$L\rho(u(\hat{\xi}, t), t)\{v(u(\hat{\xi}, t)) - V\} = \dot{m}. \tag{4.44}$$

The fact that $\dot{m} = 0$ implies that mass density ρ infinitely localizes in the singular points (sources and sinks) while vanishing elsewhere.

To close the cycle of passive treadmilling we need to regularize the problem near the singular points by cutting out small regularization domains of size ϵ around the sources and sinks and appropriately reconnecting the incoming and the outgoing flows of matter. In this way we obtain an effective 'polymerization zone' around each source $\Gamma_- = \{u \in [-1/2, 1/2] / |u - \gamma_-| < \epsilon\}$ and an effective 'depolymerization zone' around each sink $\Gamma_+ = \{u \in [-1/2, 1/2] / |u - \gamma_+| < \epsilon\}$. We assume that in the domain Γ_- the network is constantly assembled from the abundant monomers while in the domain Γ_+ it is constantly disassembled so that the pool of monomers is replenished. The ensuing closure of the treadmilling cycle is instantaneous (jump process) allowing the monomers to avoid the frictional contact with the environment. In other words, we assume that the jump part of the treadmilling cycle is a passive equilibrium process driven exclusively by myosin contraction.

In the regularized problem the mass flux

$$\dot{m} = \left(\int_{\partial\Gamma_-}^{\partial\Gamma_+} \frac{du}{v(u) - V} \right)^{-1}$$

becomes finite and the corresponding density profiles, that are now defined only outside sources and sinks, can be found using formula (4.44) with $\dot{m} \neq 0$. As in our discrete model, here we also represent the 'returning' flow by discontinuities so that a particle reaching the boundary of the sink region following a smooth trajectory (path AB in Fig. 4.8) instantly reappears on the boundary of the source region (path $B'A'$ on Fig. 4.8b).

4.2.9 Nonlinear Active Stress

The fact that the bifurcation leading to polarization and motility initiation is always a supercritical pitchfork indicates that in the present form the model does not allow for metastability and coexistence of motile and non-motile configurations [55, 153, 168]. However, to capture this effect we need to modify our model only slightly. The main idea is to consider a more realistic nonlinear dependence of the active stress on motor concentration.

To this end we rewrite the main system of equations in the form

$$\begin{aligned} -\mathscr{Z}\partial_{xx}\sigma + \sigma &= \mathscr{P}\Phi(rc)/r, \\ \partial_t c + \mathscr{K}\partial_x(c\partial_x\sigma) &= \partial_{xx}c, \end{aligned} \tag{4.45}$$

where, following [22], we set $r = c_0/c^*$ and assume that the function $\Phi(x)$ is linear at small values of x but then saturates after around $x = 1$. In computations we use a particular form of nonlinearity $\Phi(x) = x/(1+x)$.

For simplicity we first analyze the 'rigid' limit where $k \to \infty$ and $L \to L_0$ while the stress on the boundaries $-k(L/L_0 - 1)$ remains finite. Notice that in this limit, which also means that $\mathscr{P} \to 0$ and $\mathscr{K} \to \infty$, we have to re-scale the stress by $c_0\chi$ instead of k. If with some abuse of notations, we denote $\sigma := \sigma/\mathscr{P}$, the new dimensionless parameter replacing $\mathscr{K}$ and $\mathscr{P}$ will be $\lambda = c_0\chi/(\xi D) = \mathscr{K}\mathscr{P}$, see also [22, 59, 61, 67]). The mechanical boundary conditions can be written in the form $\sigma(l_\pm(t), t) = \sigma_0$ and $\dot{l}_\pm = \lambda\partial_x\sigma(l_\pm(t), t)$, where $\sigma_0 = -\lim_{\mathscr{P}\to 0}\lim_{L\to 1}(L-1)/\mathscr{P}$.

For TW solutions we can write the analogue of (4.29)

$$-\mathscr{Z}s'' + s + s_0 = \frac{\lambda}{r}\Phi\left(r\frac{\exp(s - Vu)}{\int_0^1 \exp(s - Vu)du}\right), \tag{4.46}$$

where $s = \lambda(\sigma - \sigma_0)$ and $s_0 = \lambda\sigma_0$. The boundary conditions take the form $s(0) = s(1) = 0$ and $s'(0) = s'(1) = V$. The difference with our static solutions, described in Sect. 4.2.5, is that now we have to find the stress at the boundary s_0 instead of the length L.

The analytical study of the motility initiation bifurcation in this case is presented in [126]. The numerical results are illustrated in Fig. 4.9. As we see, when the nondimensional parameter r is small, which means that we are in the linear regime, the bifurcation from static to motile regime is a supercritical pitchfork. However, at larger values of r the nature of the bifurcation changes from supercritical to subcritical. This opens an interval of metastability where both the homogeneous static state and the inhomogeneous motile state are locally stable.

In Fig. 4.10 we illustrate the effect of choosing a threshold-type dependence of contractile stress on the concentration of motors. Here we dropped the assumption that the length of the moving segment is fixed. A comparison of Fig. 4.10 with Fig. 4.7b shows that the saturation of contractile stress introduces a finite zone

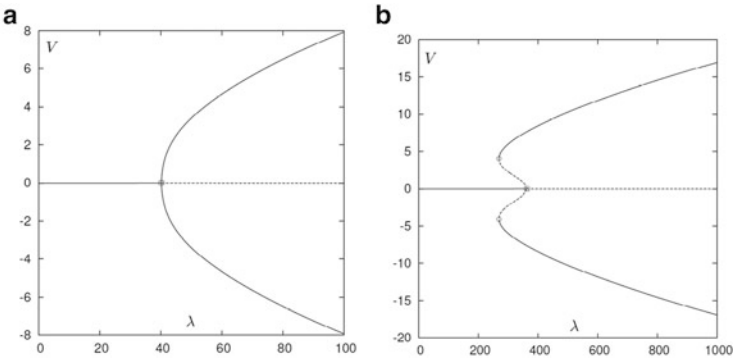

Fig. 4.9 Bifurcation diagrams in the nonlinear model with fixed length (infinite stiffness) (4.46) showing the possibility of a switch from supercritical to subcritical bifurcation. Parameters: $\mathscr{Z} = 1$. (**a**) $r = 1$. (**b**) $r = 5$

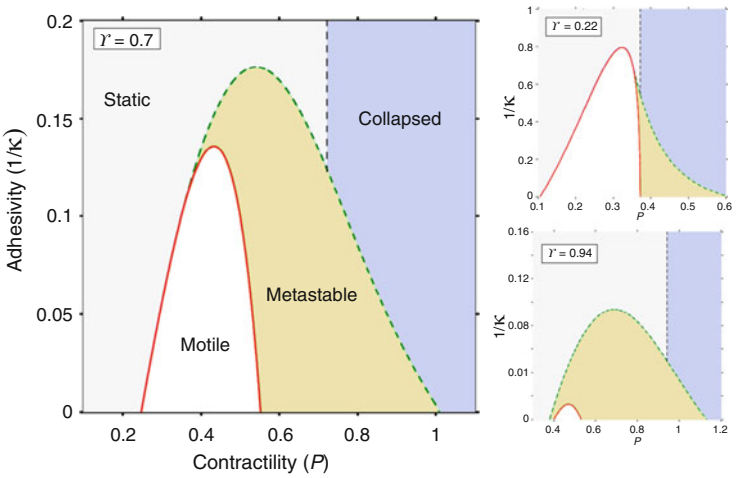

Fig. 4.10 *Left*: phase diagram in the parameter plane $(\mathscr{P}, 1/\mathscr{K})$ for the system (4.45) (with no length constraint). The parameter $\mathscr{Z}/\mathscr{K} \approx 6 \times 10^{-3}$ is fixed at its experimental value. The *solid* (*red*) line indicates the motile bifurcation threshold for the branch D_1^+ (similar to Fig. 4.7b), while the *dashed line* bounding the metastability domain indicates the location of the turning points on the motile branch in the appropriate analog of Fig. 4.9b. The *dashed line* separating static and collapsed configurations indicates the location of the turning point α in Fig. 4.3. *Right*: effects of a high (*top*) and low (*bottom*) concentration saturation thresholds

of metastability where finite perturbations are required to switch between static to a motile regimes. This prediction was recently confirmed in vivo by Barnhart et al. [14] and the metastability domain as in Fig. 4.10 was mapped experimentally. We also observe that for sufficiently large values of the saturation threshold r,

our model predicts metastability and hysteresis during both, motility initiation and motility arrest. On the arrest side [84], this prediction can be linked to the hysteresis associated with cell division [156].

4.2.10 Discussion

In this section we were mostly concerned with the discussion of the autotaxis mechanism of cell motility. The main idea is that pullers can propel the passive medium by inflicting contraction because they are themselves advected by this medium which creates an autocatalytic effect [97]. The inevitable build up of mechanical gradients in these conditions is limited by diffusion which resists the runaway and provides the negative feedback. After the symmetry of the static configuration is broken in the conditions where matter can circulate, the resultant contraction-driven flow ensures the perpetual renewal of the network and then frictional interaction with the environment allows for the steady translocation of the cell body.

A prototypical model presented in this section provides an alternative qualitative explanation of the experiments of Verkhovsky et al. [159], Yam et al. [167] that have been previously interpreted in terms of active polymerization inducing the growth of actin network [20]. Most strikingly, the predictions of this model are also in quantitative agreement with experimental data presented in [159], see [126] for a detailed comparison. This is rather remarkable in view of a schematic nature of this model and the absence of fitting parameters. The model also captures a durotactic effect since the directional motion cannot be initiated if friction with the substrate is larger than a threshold value. Below this threshold, motile regimes exist in a finite range of contractility. This means that if the cell is already in motion, it can recover the symmetric (static) configuration either by lowering or by increasing the amount of operating motors. The possibility of cell arrest under the increased contractility should be investigated in focused experiments.

We have also shown that when the contractility depends on the motor concentration nonlinearly, the system exhibits a metastability range where both static and motile regimes are stable and can coexist. In the corresponding interval of parameters a mechanical perturbation may be used to switch back and forth between static and dynamic regimes. This prediction of the model is particularly important in the context of collective cell motility (in tissues) where contact interactions are able to either initiate or terminate the motion [1, 62, 155, 158].

4.3 Protrusion

In this section we introduce a new active mechanism, polymerization-induced protrusion, and search for conditions when it can overshadow active contraction and become the main driver of self-propulsion. To maintain analytic transparency

we simplify the description of contraction by disabling the autotaxis mechanism and assuming that the distribution of motors is uniform in space and constant in time.

The crucial observation, justifying the introduction of a protrusion-centered motility mechanism, is that eukaryotic cells do not only self-propel and carry cargoes by pulling, but can also exert forces on obstacles performing mechanical pushing. However, it is quite clear that pushing cannot be accomplished efficiently by contraction only. In other words, pullers must pull while pushing should be delegated to pushers.

In this section we show that protrusion dominated motility, performed largely by pushers, may have a very particular macroscopic signature: the concavity of the force velocity relation. We also show that pulling can be also driven exclusively by protrusion but only for small values of the pulling force: it must be necessarily replaced by contraction-centered mechanism when the pulling force is sufficiently large. The substitution of one mechanism by another with increasing load is manifested by a more complex convex-concave structure of the force velocity relation. Most interesting, our model suggests that competition between protrusion and contraction can produce negative mobility in a biologically relevant range.

Viewed more broadly, the results of this section illustrate the possibility of active readjustment of the force generating mechanism in response to changes in the dipole structure of external forces showing that if necessary 'pushers' can replace 'pullers' and visa versa.

4.3.1 The Model

To model a loaded self-propelling active fragment we maintain the force balance equation (4.17) but modify the mechanical boundary conditions and write

$$\sigma(l_{\pm}(t), t) = q_{\pm}.$$

In our notations $q_+ < 0$ corresponds to pushing (at the front) and $q_- > 0$ to pulling (at the rear). In this description the mean-field elasticity has been omitted given that active protrusion provides an independent mechanism of maintaining a particular 'cell volume' (see more about this below). It will also be convenient to define the resultant force

$$Q = q_- - q_+ \geq, 0$$

which we assume to be positive and acting against the polarization direction induced by protrusion. We also introduce the force asymmetry factor

$$\epsilon = \frac{q_- + q_+}{Q},$$

which characterizes the first moment of the external force distribution. We notice that $-1 \leq \epsilon \leq 1$ with $\epsilon > 0$ corresponding to pulling and $\epsilon < 0$—to pushing.

The protrusive 'force' in our model will be introduced implicitly through the new kinematic constraints on the unknown functions $l_+(t)$ and $l_-(t)$ [75, 83, 86, 122, 131]

$$\dot{l}_\pm = v(l_\pm(t), t) + v_\pm. \tag{4.47}$$

Here $v_+ > 0$ and $v_- > 0$ are the polymerization and the depolymerization velocities, respectively. While there is considerable experimental evidence that active polymerization is indeed localized at the leading edge of a crawling cell, the de-polymerization may be spread along the length of the lamellipodium [75, 131]. However, in the interest of analytic transparency, such spreading will be ignored in this study (see the analysis of this assumption in [122]).

Observe that our assumption (4.47) implies that there is a nonzero (negative) mass flux going through the system

$$\dot{m} = -\rho(l_\pm(t), t)v_\pm.$$

To account for this flux we need to slightly modify the theoretical framework introduced in the first section, in particular, (4.9) has to be modified since there is now an incoming and outcoming fluxes of free energy associated with production polymerized monomers at the front and dissociating the filaments into free monomers at the rear. By following the same steps as in the first section we obtain

$$R = \int_{l_-}^{l_+} (\sigma \partial_x v + \nu A + J\partial_x \mu)dx - \dot{m}\Delta\mu, \tag{4.48}$$

where $\Delta\mu = [f + p/\rho]_-^+$ is the driving force of active treadmilling. Since for our infinitely compressible gel the thermodynamic pressure $p = 0$ we obtain $\Delta\mu = f(l_+(t)) - f(l_-(t))$. A knowledge of polymerization/depolymerization reaction kinetics can provide us with the kinetic relation whose simplest form would be $\dot{m} = \psi(\Delta\mu)$ and then we also need to specify the externally (for our model) imposed driving force $\Delta\mu$. However, to maintain the decoupling between the force balance problem and the mass transport problem, secured by our infinite compressibility assumption, we define protrusion by prescribing two other pieces of information: the kinematic variables $v_\pm$.

In fact, it will prove natural to work with a slightly different set of parameters. Thus, parameter

$$V_m = \frac{v_- + v_+}{2} \geq 0$$

prescribes polarity of the cell and provides the scale of the maximal velocity. The remaining kinematic parameter

$$\Delta V = v_+ - v_-,$$

introduces the asymmetry between polymerization and de-polymerization and, as we show below, quantifies the degree of engagement of the contractile mechanism.

The other constitutive hypotheses will be as in the previous section except that we assume for simplicity that in the transport of motors diffusion dominates drift and $c(x,t) \equiv c_0$. Then the contraction-generated pre-stress is also constant $\chi_0 = aA_0c_0 > 0$, which is a rather usual assumption in the models of active gels [75, 83]. Notice that in the previous section we used the notation χ for contractile pre-stress per unit motor mass which is now irrelevant since c does not depend on either space or time.

If we now normalize length by $\sqrt{\eta/\xi}$, time by η/χ_0 and stress by χ_0, we obtain a free boundary problem which depends on four dimensionless parameters.

$$\begin{aligned} -\partial_{xx}\sigma + \sigma &= 1 \\ \sigma(l_\pm(t),t) &= q_\pm \\ \dot{l}_\pm &= v_\pm + \partial_x\sigma(l_\pm(t),t). \end{aligned} \tag{4.49}$$

The linear force balance equation with mechanical boundary conditions can be integrated (see [75, 83] for the case without cargo) and we obtain

$$v(x,t) = \frac{A_-\cosh(l_-(t)-x) + A_+\cosh(l_+(t)-x)}{\sinh(l_+(t)-l_-(t))}, \tag{4.50}$$

where

$$A_\pm = \pm(1 - Q(\epsilon \pm 1)/2). \tag{4.51}$$

Knowledge of the velocity field and the use of kinematic boundary conditions allows one to obtain a closed dynamical problem for the total length $L(t)$

$$\dot{L} = \Delta V + (\epsilon Q - 2)\tanh\left(\frac{L}{2}\right). \tag{4.52}$$

After this equation is solved the position of the geometrical center of the cell $G(t)$ can be found by direct integration from

$$\dot{G} = V_m - \frac{Q}{2\tanh(L/2)}. \tag{4.53}$$

To specify solutions of (4.52) and (4.53) we need to supply the initial conditions $L(0)$ and $G(0)$ that also fix the initial velocity profile through (4.50).

We are interested in traveling wave (TW) solutions of (4.52) describing steadily translocating active fragments. The corresponding critical points of (4.52) exist if and only if

$$0 < \Delta V < 2 - \epsilon Q. \tag{4.54}$$

When these conditions are satisfied the length stabilizes as $t \to \infty$ at the value

$$L = 2\tanh^{-1}\left(\frac{\Delta V}{2-\epsilon Q}\right) > 0.$$

4.3.2 Force Velocity Relation

Notice that at $t \to \infty$ the function $\dot{G}$ converges to a constant V given by the force-velocity relation

$$V = V_m - \frac{Q}{\Delta V} + \frac{\epsilon Q^2}{2\Delta V}. \tag{4.55}$$

In our notations the fragment moves to the right against the load if $V > 0$ and is dragged backwards by the load if $V < 0$. The maximum velocity $V^* = V_m$ is achieved when there is no load $Q = 0$ and the corresponding reference length will be denoted by $L^* = L(Q = 0)$. Since the TW regimes are stable only if $2-\epsilon Q > 0$, pushing ($\epsilon < 0$) contributes to stability while pulling ($\epsilon > 0$) plays a destabilizing role.

At $\Delta V = 0$ the loaded fragment shrinks to a point while at $\Delta V = 2 - \epsilon Q$ its length diverges. For singular solutions with $L = \infty$ which are only relevant in the case of pulling, the force velocity relation can be extended beyond the singularity formation threshold as

$$V = V_m - Q/2. \tag{4.56}$$

The full force-velocity relation in the (V, Q) plane including both regular and singular solutions is illustrated in Fig. 4.11a, b. One can see that it is markedly different for $\epsilon > 0$ (pulling) and $\epsilon < 0$ (pushing). The main feature distinguishing pushing from pulling is the curvature of the force velocity relation which in the regular regimes (4.55) is given by $\partial^2 V/\partial Q^2 = \epsilon/\Delta V$, and in the singular (pulling) regimes by $\partial^2 V/\partial Q^2 = 0$. One can also see that the curvature is always negative in pushing regimes with $\epsilon < 0$ which means that the corresponding force velocity relation is concave. Under pulling loads with $\epsilon > 0$ the force velocity curve is convex for regular regimes and is linear for singular regimes.

In the pushing regimes the force velocity curve is characterized by the stall force $Q^* = (1 - \sqrt{1 - 2\epsilon\Delta V V_m})/\epsilon$ and the maximum velocity $V^* = V_m$, see Fig. 4.11b. The concavity of the force velocity relation in this case agrees with experiments [26, 115, 135, 170]. In the case of pulling, the force-velocity relation is convex for $Q < Q_c = (2 - \Delta V)/\epsilon$, where $L < \infty$ and is linear for $Q > Q_c$, where $L = \infty$, see Fig. 4.11a. In the convex range the function $V(Q)$ is non-monotone when $\Delta V < 1$ and one can distinguish two regimes: the branch $Q < Q_n = 1/\epsilon$ where the mobility is positive, $V(Q) \sim V_m - Q/\Delta V$, and, as we show below,

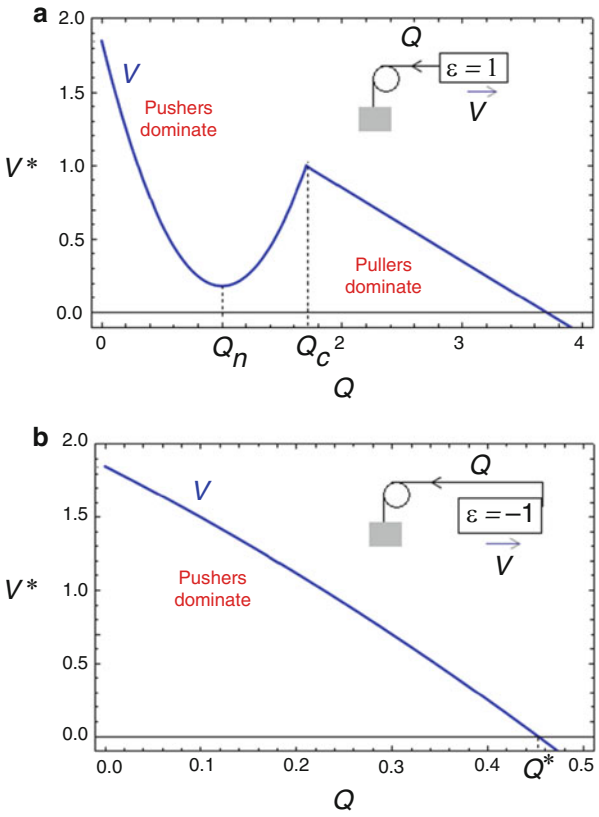

Fig. 4.11 The typical force-velocity relations in pure pulling (**a**) and pushing (**b**) regimes

protrusion dominates, and the branch $Q_c > Q > Q_n$ where the mobility is negative, $V(Q) \sim \epsilon Q^2/(2\Delta V)$ and the dominant active mechanism is contraction. Along the negative mobility branch the cell elongates to support larger loads till the length diverges at a critical value $Q = Q_c$. Beyond this value, we obtain configurations with infinitely separated boundary layers and mobility becomes again positive. The associated density profiles are discussed in [122].

The observed differences in the structure of force velocity relations in the regimes of pushing and pulling can be interpreted in terms of the competition between pushers and pullers. We begin with an observation [33, 83] that the analysis of the global force balance, $L\int_{-1/2}^{1/2} v(u)du = -Q$, does not allow one to distinguish between pushing and pulling. To identify the role of different active agents we need to consider the balance of couples where an important role is played by the sign of the dipole component of the applied load.

By multiplying the force balance equation (4.49) in the TW regime by u and integrating over the body of the cell we obtain

$$\frac{\epsilon}{2}Q - L\int_{-1/2}^{1/2} uv(u)du = \int_{-1/2}^{1/2} \sigma(u)du. \tag{4.57}$$

The first term in the left hand side $T_e = \frac{\epsilon}{2}Q$ is the moment of external forces. Since we assumed that $Q > 0$, pulling is associated with a positive applied dipole while pushing—with a negative applied dipole. The second term on the left hand side $T_f = -L\int_{-1/2}^{1/2} uv(u)du$ represents frictional dipole which may have different signs. The integral on the right hand side defines the active dipole which can be also rewritten as $T_a = \int_{-1/2}^{1/2}(1 + L^{-1}\partial_u v)du$. This term can be further decomposed into the sum $T_c + T_p$ where contraction component is $T_c = 1 > 0$ and protrusion component is $T_p = -\Delta V/L < 0$. The opposite signs of these two terms suggest that the underlying active mechanisms are inherently different: the protrusion term represents distributed pushers while the contraction term represents distributed pullers [132, 144].

Due to the presence of a contraction (positive) force dipoles the rear boundary of the cell is pulled forward while the front boundary is pulled backward. As a compensation, contraction produces internal retrograde flow at the rear and pro-grade flow at the front. In contrast, protrusion (negative) force dipole pushes the rear of the cell backward while the front of the cell is pushed forward. This is compensated internally by retrograde flow at the front and pro-grade at the rear. These flows must be superimposed with the mean flow $\bar{v} = -Q/L$ which is associated solely with the total applied force and is therefore always retrograde.

It is now natural to identify the point Q_n in Fig. 4.11a with a crossover from pushers dominated to pullers dominated regimes. This interpretation is supported by comparing the magnitudes of the two competing active couples. The observed crossover correlates with the transition from positive to negative mobility which also takes place at Q_n. Negative mobility has been discussed previously in the context of individual [38, 57, 94, 130] and interacting [25, 110] Brownian motors. The regimes where velocity of the crawling cell increases with an opposing pulling force at the rear have been envisioned in [72] where negative mobility was attributed to the coupling between the velocity of retraction and the applied force $v_-(Q)$ [113]. In our model such coupling is absent which shows that negative mobility may also have a different origin. The parameter estimates showing that negative motility is realistic in physiological conditions can be found in [122].

4.3.3 Elastic Regularization

The obtained force-velocity relations are not fully satisfactory because some of the solutions have diverging length. A natural way to regularize such singular solutions

is to introduce an intermediate-time stiffness of the cell. Such stiffness, which we have already encountered in the previous section, can in some regimes prevent cells from contraction-induced collapse, it sets the rest length and it may also keep this length from diverging in the case of super critical pulling. Time dependent visco-elastic properties of the cytoskeleton [21, 37, 101] are usually incorporated either in the framework of a short time (Maxwell) elastic model [28, 73, 75, 121, 131] or a long time (Kelvin–Voigt) elastic model [10, 86, 111].

The simplest purely elastic regularization, already considered in the previous section, is through mean field coupling between the leading and trailing edges of a cell [12, 49, 117, 142]. If this coupling is linear elastic, the applied loads become

$$q_\pm \to q_\pm + k\frac{L-L_0}{L_0},$$

where $k > 0$ is a dimensionless stiffness and L_0 is a prescribed dimensionless reference length (for the comparison with models of bulk linear elasticity, see [122]). The meaning of parameter L_0 is clear from the fact that for $k > 1$ and $V_m = \Delta V = 0$ there exists a nontrivial static solution with $L = L_0(1 - 1/k)$ (preferred length).

In dynamics the steady state (TW) solution is now stable for all $\Delta V > 0$ and to find $L(Q)$ one needs to solve

$$\Delta V = \left(2 - \epsilon Q + 2k\frac{L-L_0}{L_0}\right)\tanh\left(\frac{L}{2}\right).$$

Then, the force velocity relation can be found from the relation

$$V(Q) = V_m - \frac{Q}{2\tanh\left(\frac{L(Q)}{2}\right)}.$$

The k dependence of the force velocity relation is illustrated in Fig. 4.12. We observe that independently of the value of k all force-velocity curves cross at $Q = 0$ where $V = V^*$. The second common intersection point is at

$$Q_I = \frac{1}{\epsilon}\left(2 - \frac{\Delta V}{\tanh\left(\frac{L_0}{2}\right)}\right).$$

As we see, at $k \to 0$ the mean field force-velocity curves approach their minimal model counterparts including both the regular regimes with finite cell lengths and the singular regimes with infinite cell lengths. However, despite similarity in shape between the force velocity curves in the minimal model and in the regularized model with $k \sim 0$, the length of the cell in the regularized model is always *finite* so that infinite stretching, undermining the minimal model, does not take place.

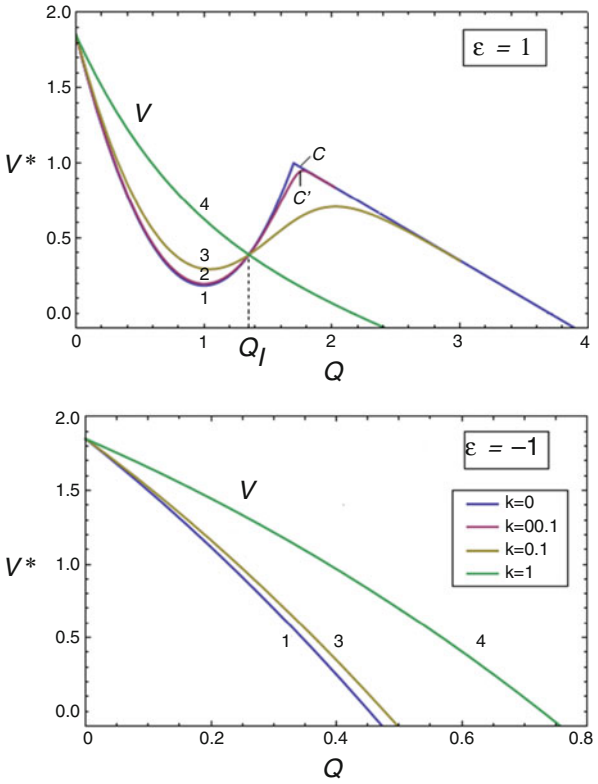

Fig. 4.12 Force velocity relations in pure pushing and pulling modes with different $k_{1,2,3,4} = \{0, 0.01, 0.1, 1\}$ and $L_0 = 1$. Driving parameters are $v_- = 1.7$ and $v_+ = 2$. The minimal model is recovered at $k = 0$

The phenomenon of negative mobility for the pulled cells survives in the mean field model and disappears only at a critical value of the stiffness $k = k^*(\Delta V)$, see Fig. 4.13. The qualitative difference in convexity between pulling and pushing persists beyond $k^*(\Delta V)$, see for instance regime with $k = 1$ in Fig. 4.12. However, at $k \gg k^*(\Delta V)$ the force-velocity relations associated with pushing and pulling regimes become similar.

To check robustness of these predictions we studied in [122] three different extensions of this model allowing for inhomogeneous friction, bulk depolymerization and density dependent contractile pre-stress. Our analysis shows that for all these augmented models our main conclusion about the difference in convexity properties between the force velocity curves in pushing and pulling regimes remain valid.

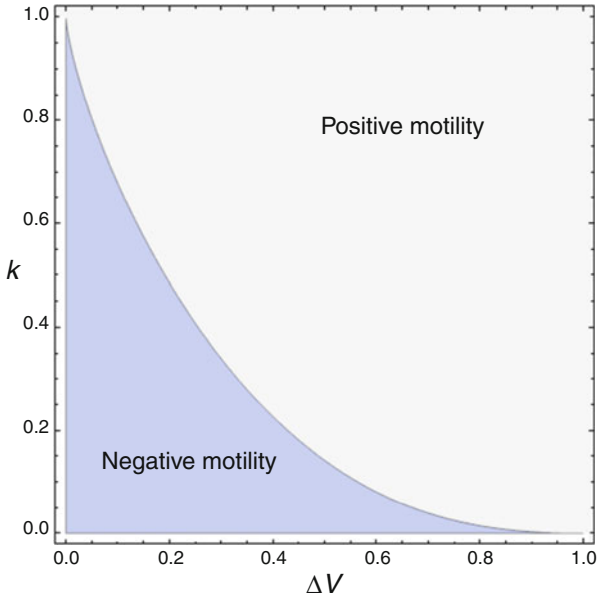

Fig. 4.13 Domain of negative mobility in the parameter space $(k, \Delta V)$. The boundary between regimes with positive and negative mobility is given by the function $k = k^*(\Delta V)$

4.3.4 Alternative Driving Modes

So far we have been using an assumption that protrusion is driven by the kinematic fluxes characterized by parameters v_+, v_- or $V_m, \Delta V$. According to this assumption, illustrated in Fig. 4.14, we impose separately the velocities of polymerizing (arriving) and de-polymerizing (departing) mass points, see also [75, 83, 86, 102, 131]. The fact that nothing has been said about the densities of the arriving or departing material allows one to decouple the mechanical problem from the mass transportation problem. The resulting analytic transparency, however, comes at a cost.

First, it is clear that active treadmilling in our model is characterized by only one parameter, the mass flux $\dot{m}$, so by fixing two parameters V_m and ΔV we are implicitly constraining both treadmilling and contraction. This is also clear from the fact that parameter $\Delta V = v_+ - v_-$ serves as a measure of (dimensionless) energy consumption in the contraction mechanism $P_c = -\int_{l_-}^{l_+} \partial_x v > 0$. Indeed, for the TW regimes the integral terms can be computed explicitly giving $P_c = \Delta V$.

Second, by prescribing the kinematic fluxes v_+ and v_- we have no direct control of the treadmilling mass flux. As a result we encounter singular regimes with $\dot{m} = 0$ which leads to either infinite mass localization inside the cell [122]. Third, by focusing on kinematic fluxes we do not put any restrictions on the energy consumption required to sustain different active mechanisms which appears to be a natural biological constraint.

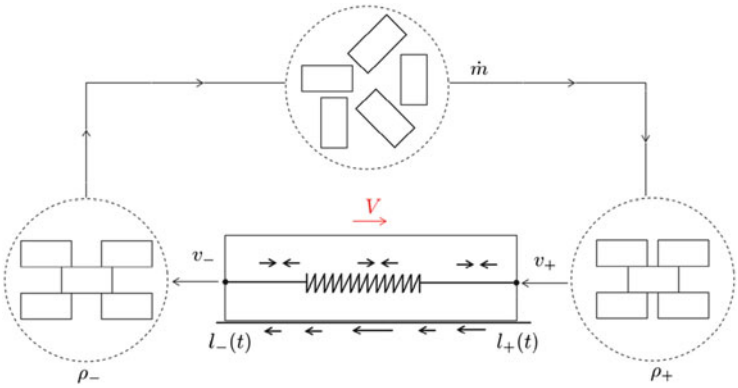

Fig. 4.14 Schematic structure of the treadmilling cycle showing different densities of arriving (polymerizing) and departing (depolymerizing) material

Notice also that the problem setting where driving is performed through parameters v_+ and v_- contains an implicit assumption that the material arrives with a particular density (particular structural organization). Another implicit assumption is that the departing material has a density which depends on the activity of the contractile machinery. While these assumptions are plausible, they may not be the most natural ones from the biological point of view.

In view of these limitations of the model with kinematic driving, it is instructive to consider an alternative modality of driving by imposing constraints on energetic parameters. The main difficulty in dealing with non kinematic driving schemes is that they couple the mechanical and the mass transport problems already in the minimal setting.

Assume, for instance, that the cell controls the treadmilling rate, characterized by the total mass flux $\dot{m} < 0$, and the energetics of the contraction process, characterized by the consumed power $P_c = \Delta V$. The advantage of this new parametrization is that protrusion and contraction can now be controlled independently.

If we choose the pair $(\dot{m}, P_c)$ as the parameters instead of $(V_m, \Delta V)$, we again obtain stable TV solutions given that $P_c < 2 - Q\epsilon$ and $\dot{m} < 0$. The proposed driving mode is in fact equivalent to the kinematic driving mode in the TW regimes because the Jacobian of the transformation $(v_-, v_+) \to (P_c((v_-, v_+)), \dot{m}(v_-, v_+))$

$$\det \begin{pmatrix} \frac{\partial P_c}{\partial v_-} & \frac{\partial \dot{m}}{\partial v_-} \\ \frac{\partial P_c}{\partial v_+} & \frac{\partial \dot{m}}{\partial v_+} \end{pmatrix} = \frac{\int_{-1/2}^{1/2} \frac{du}{(v(u)-V)^2}}{L(\int_{-1/2}^{1/2} \frac{du}{v(u)-V})^2} \geq \frac{1}{L}$$

is strictly positive for $0 < L < \infty$.

In Fig. 4.15 we show the force velocity relations in the minimal model with prescribed $(\dot{m}, P_c)$. One can see that the qualitative difference between pushing and pulling endures in this new setting, moreover, we again observe regimes with

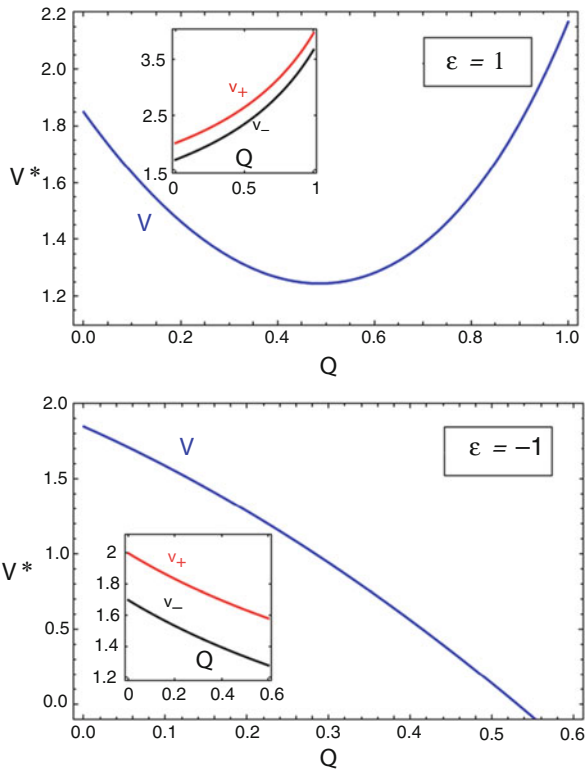

Fig. 4.15 Force velocity relations in pure pushing and pulling TW regimes when driving is performed by imposing $\dot{m} = -6.1$ and $P_c = 0.3$. *Insets* show the ensuing dependencies of v_+ and v_- on Q

negative mobility. It is interesting that by fixing parameters P_c and $\dot{m}$ we induce a dependence of the polymerization and depolymerization rates (v_-, v_+) on Q (see the inserts in Fig. 4.15) which agrees qualitatively with the trends suggested in [83] based on the polymerization ratchet model. We also note that at sufficiently strong pulling loads $Q > Q_c = (2 - P_c)/\epsilon$, the cell length L diverges which suggests that also in the case of non-kinematic driving the minimal model should still be elastically regularized.

Ultimately, the choice of the driving mode requires microscopic modeling and the answer may depend on the type of the cell, the environment and the regime of loading.

4.3.5 Discussion

In this section we studied an interplay between contraction and protrusion required to sustain and carry various cargoes. By using an analytically transparent framework we demonstrated that contraction and protrusion mechanisms can interchange their roles as one varies the dipole component of the external load.

Our model predicts a possibility of a sharp transition between protrusion dominated motility and contraction dominated motility in response to an increase of the pulling force. This transition has a macroscopic signature and can be in principle identified experimentally with a negative mobility range on a force-velocity curve. Vis-à-vis the general behavior of active media, we have shown that an interplay between 'pushers' and 'pullers' can lead to observable effects in the presence of applied loads. The importance of the idea that different active mechanisms can swap roles depending on the task goes far beyond the subject of cell motility.

While our minimal model still under-represents some physical effects (e.g. autotaxis of myosin motors, active adhesion, complex membrane dynamics, etc. [48, 63, 141, 163, 165, 166, 169]) it allows one to go beyond force velocity relations and study the efficiency of cargo-pulling machinery. Thus, in [122] we have shown that a competition between protrusion and contraction can result in a bi-modal structure of the load-efficiency relation.

Perhaps our most intriguing finding is that the fine structure of the force-velocity relation may depend on the modality of external driving and we argued that kinematic driving may not be the only physically and biologically natural choice. In particular, we suggested that instead of the rates of polymerization and depolymerization, the cell may be controlling the energy supplies required for the functioning of contraction and protrusion mechanisms. We have shown, however, that while the detailed shape of the force velocity relation depends on the choice of the driving mode, its loading-sensitive convexity-concavity structure is a robust feature of the model.

4.4 Adhesion

In this section we turn our attention to adhesion. We remain in the general framework developed in the previous sections, see also [2, 44, 65, 83, 102, 124, 127, 146, 160], and study the active re-organization of adhesive complexes inside a self-propelling layer ensuring an optimal cost-performance trade-off for steady self propulsion. We assume that (in the range of interest) the energetic cost of self-propulsion is velocity independent (cf. [125]) and adopt, as an optimality criterion, the maximization of the overall velocity. We are interested in steady translocation and assume that the internal distributions of mechanical parameters are compatible with the traveling wave ansatz. This simplifying assumption allows us to replace the optimization of the crawling stroke in space and time by a purely spatial optimization of the internal distribution of active elements in the co-moving coordinate system. In a similar but simpler setting the dependence of cell velocity on the distribution of adhesion properties was first studied by Carlsson [33].

Our main result is that depending on the outcome of the competition between contraction and protrusion mechanisms, the 'optimal' adhesion would cooperate either with one or the other.

4.4.1 The Model

Since our knowledge of the mechanism controlling the transport and the intensity of active agents performing adhesion is rather limited, we adopt in this section a semi-kinematic approach and treat the corresponding distribution as a functional control parameter constrained by the fundamental mechanical balances. We then pose a variational problem of finding the optimal temporal and spatial distributions of this control parameter inside a crawling continuum body. In view of some successful attempts to justify such reverse engineering approach [125], we anticipate that our optimal solutions will be eventually backed by an appropriate constitutive theory describing active adhesive clusters.

The object of our study is again a one-dimensional segment of viscous active gel representing the cell lamellipodium on a frictional substrate. The force balance will be still written in the form (4.17) but we now assume that the frictional coefficient, mimicking the distribution of focal adhesions, is space and time dependent $\xi(x,t) \geq 0$. We also now assume that the active pre-stress $\chi_0(x,t) \geq 0$ is a function of space and time, however, instead of writing an equation for $c(x,t)$ we view the function $\chi_0(x,t)$, entering the constitutive law $\sigma = \eta\partial_x v + \chi_0$, as an independent functional degree of freedom.

We further assume that some internal mechanism (stiffness of the cell cortex [12, 21, 49, 93, 117, 142], osmotic pressure actively controlled by the channels and pumps on the cell membrane [69, 147], etc.) maintains a given size $L(t) = L_0$ of the cell (the 'rigid' model briefly discussed in Sect. 4.2.9). To model active protrusion we again impose the two kinematic Stefan type boundary conditions (4.47).

The two functions $\chi_0(x,t)$ and $\xi(x,t)$ will be interpreted as infinite dimensional controls parameters and found through an optimization procedure. Even in the absence of a detailed microscopic model governing the rearrangement of these agents we still need to subject them to integral constraints prescribing the average number of adhesion complexes [13]

$$\frac{1}{L}\int_{l_-(t)}^{l_+(t)} \xi(x,t)dx = \xi^*, \tag{4.58}$$

where $\xi^* > 0$ is a given constant and

$$\frac{1}{L}\int_{l_-(t)}^{l_+(t)} \chi_0(x,t)dx = \chi^*, \tag{4.59}$$

where $\chi^* > 0$ is another given constant representing the average number of contractile motors [150]. It is clear from (4.58), (4.59) that since we prescribe the density of active agents, the performance of the self-propulsion machinery will be proportional to the length of the active segment, so the appropriate velocity functional must be also normalized by the total length.

To simplify the analysis we assume that the motion of the active segment is steady [75, 131] with unknown velocity $V = \dot{l}_- = \dot{l}_+$ and that the unknown functions σ, v and the unknown controls ξ, χ depend exclusively on the co-moving coordinate u. Then in dimensionless variables $\sigma := \sigma/\chi^*$, $x := x/\sqrt{\eta/\xi^*}$, $t := t/(\eta/\chi^*)$, $\xi := \xi/\xi^*$ and $\chi := \chi/\chi^*$ we obtain the force balance equation

$$-\frac{1}{L^2}\partial_u\left(\frac{\partial_u\sigma(u)}{g_1(u)}\right) + \sigma(u) = g_2(u). \tag{4.60}$$

The re-scaled control functions

$$g_1(u) = \xi(Lu) \geq 0, g_2(u) = \chi_0(Lu) \geq 0$$

must satisfy the constraints

$$\int_{-1/2}^{1/2} g_1(u)du = \int_{-1/2}^{1/2} g_2(u)du = 1. \tag{4.61}$$

The boundary conditions take the form

$$\begin{cases} \sigma(-1/2) = \sigma(1/2) \\ \frac{1}{L^2}\left(\frac{\partial_u\sigma(1/2)}{g_1(1/2)} - \frac{\partial_u\sigma(-1/2)}{g_1(-1/2)}\right) = -\overline{\Delta V} \end{cases}, \tag{4.62}$$

where

$$\overline{\Delta V} := \frac{\Delta V}{L}.$$

The dimensionless velocity of the segment per length $\overline{V} = V/L$ can be found from the formula

$$\overline{V} = \overline{V_m} + \frac{1}{2L^2}\left(\frac{\partial_u\sigma(1/2)}{g_1(1/2)} + \frac{\partial_u\sigma(-1/2)}{g_1(-1/2)}\right), \tag{4.63}$$

where

$$\overline{V_m} := \frac{V_m}{L}.$$

If we now assume that the two parameters $(\overline{V_m}, \overline{\Delta V})$, characterizing actin treadmilling, are fixed we can pose the optimization problem of finding the controls $g_1(u)$, $g_2(u)$ ensuring the maximization of the normalized velocity $\overline{V}$. This problem is nontrivial because the functional $\overline{V}\{g_1, g_2\}$ is prescribed implicitly through the unknown solution of the boundary value problem (4.60), (4.62). To our advantage this linear elliptic problem is classical, e.g. [100].

We observe that parameter $\overline{V_m}$ enters the expression for the velocity (4.63) in an additive way and does not affect the solution of the optimization problem. The reason is that $\overline{V_m}$ characterizes a propulsion mode associated with simple accretion of the material at the front and its simultaneous removal at the rear; when $\overline{V_m} \neq 0$ an a priori polarity is imposed and the problem of motility initiation disappears. In view of the complete independence of this mode of self-propulsion from our controls, we assume without loss of generality that $\overline{V_m} = 0$.

In contrast to $\overline{V_m}$, the second parameter $\overline{\Delta V}$, also characterizing the protrusion strength, does not induce polarity. As we have seen in the previous section, this parameter represents the mechanical action of pushers. Indeed, consider again the global balance of couples in the co-moving coordinate system [see also (4.57)]

$$L\int_{-1/2}^{1/2} g_1(u)v(u)udu - \sigma_0 = -\overline{\Delta V} + \int_{-1/2}^{1/2} g_2(u)du. \tag{4.64}$$

Here the first term in the left hand side $-T_f = L\int_{-1/2}^{1/2} g_1(u)v(u)udu$ characterizes the total moment due to external (frictional) forces [137] and the second term $T_r = \sigma_0$ corresponds to passive reaction forces resulting from the prescription of the length of the segment. The first term in the right hand side $-T_p = T = \overline{\Delta V}$ is due to active protrusion, while the second term $T_a = \int_{-1/2}^{1/2} g_2(u)du = 1$ is due to active contraction. Our assumption that $\overline{\Delta V} > 0$ means that the protrusion couple has a negative sign showing that the corresponding force dipoles act on the surrounding medium by pushing outward and creating negative stress. Instead, the contraction couple has a positive sign because the contractile forces pull inward and the induced stresses are positive. We can therefore (tentatively) argue that motility is protrusion-dominated when $T > 1$ and it is contraction-dominated when $0 < T < 1$. This assertion will be supported in what follows by rigorous analysis.

4.4.2 Contraction Driven Motility

The simplest analytically transparent case is when protrusion is disabled $\overline{\Delta V} = 0$ and motility is fully contraction-driven.

Suppose first that $g_1 \equiv 1$ which means that the adhesion complexes are distributed uniformly. Then the velocity can be expressed as a quadrature

$$\overline{V} = -\frac{1}{2\sinh(\frac{L}{2})}\int_{-1/2}^{1/2} \sinh(Lu)g_2(u)du \tag{4.65}$$

here again we see that if the function $g_2(u)$ is even, then $\overline{V} = 0$ (analog of Purcell's theorem [87, 119]). If the distribution $g_2(u)$ is non-symmetric and, for instance, more motors are placed at the rear of the segment, the velocity will become positive.

Using the fact $g_2(u) \geq 0$ we can also conclude from (4.65) that $\overline{V} \leq 1/2$. This upper bound is reached when all the motors are fully localized at the rear and $g_2(u) = \delta(u + 1/2)$.

Now, consider the general case when the focal adhesions are distributed inhomogeneously: $g_1(u) \neq$ const. Since (4.60) is a Sturm–Liouville problem, its solution can be written as

$$\sigma(u) = \sigma_0 - \int_{-1/2}^{1/2} G(u,s)\,[g_2(s) - \sigma_0]\,ds, \tag{4.66}$$

where the Green's function $G(u,s)$ can be represented by two auxiliary functions $h(u)$ and $f(u)$

$$G(u,s) = \frac{1}{C}\left[h(u)f(s)\mathbf{1}_{[s<u]} + h(s)f(u)\mathbf{1}_{[u<s]}\right], \tag{4.67}$$

solving the following standard boundary value problems [100]:

$$\begin{cases} (\frac{1}{g_1}h')' = L^2 h \\ h(-1/2) = 1, h(1/2) = 1 \end{cases}, \quad \begin{cases} (\frac{1}{g_1}f')' = L^2 f \\ f(-1/2) = 1, f(1/2) = -1 \end{cases}. \tag{4.68}$$

In (4.67), $C = (hf' - fh')/g_1$ is a constant involving the Wronskian of the two auxiliary functions $h(u)$ and $f(u)$ and $\mathbf{1}$ is the indicator function. We can now write

$$\overline{V} = \frac{1}{2}\int_{-1/2}^{1/2} f(u)(g_2(u) - \hat{g}_2)du, \tag{4.69}$$

where we introduced a new measure of inhomogeneity of contraction:

$$\hat{g}_2 = \frac{\int_{-1/2}^{1/2} h(u)g_2(u)du}{\int_{-1/2}^{1/2} h(u)du}.$$

If both functions $g_{1,2}(u)$ are even, then $f(u)$ is odd and, since the integral of a product of an odd and an even functions is equal to zero, we obtain that $\overline{V} = 0$. The same result follows if we assume that contraction is homogeneous $g_2(u) = \hat{g}_2 = 1$ while the adhesion distribution $g_1(u)$ is arbitrary. Therefore, to ensure motility at $\overline{\Delta V} = 0$, contraction must be inhomogeneous while adhesion may still be uniform (provided contraction is not even).

To find the optimal distributions $g_1(u)$, $g_2(u)$ we proceed in two steps. We first show that $\overline{V} \leq 1$ and then find a configuration of controls allowing the cell to reach this bound.

Notice that we can rewrite (4.69) in the form

$$\overline{V} = \frac{1}{2}\left(\int_{S_+} f(u)(g_2(u) - \hat{g}_2)du + \int_{S_-} f(u)(g_2(u) - \hat{g}_2)du\right),$$

where we defined the domains $S_- = \{u/g_2(u) \leq \hat{g}_2\}$ and $S_+ = \{u/g_2(u) > \hat{g}_2\}$. Applying the maximum principle to (4.68) we obtain that $1 \geq h(u) \geq 0$ and $h(u) \geq f(u) \geq -h(u)$. Using the bounds on f, we can write

$$\overline{V} \leq \frac{1}{2}\left(\int_{S_+} h(u)g_2(u)du + \hat{g}_2 \int_{S_-} h(u)du\right).$$

Since the integrands are positive and $h(u) \leq 1$ it finally follows that

$$\overline{V} \leq \int_{-1/2}^{1/2} h(u)g_2(u)du \leq \int_{-1/2}^{1/2} g_2(u)du = 1. \tag{4.70}$$

Observe that in the case of a homogeneous adhesion, the velocity could reach only one half of this maximal value.

We now show that the maximal value of velocity $\overline{V} = 1$ can be reached if both controls $g_1(u)$ and $g_2(u)$ are fully localized. Take $\theta > 0$ and consider a regularized distribution

$$g_1(u;\theta) = \frac{1}{\pi}\frac{\theta}{\theta^2 + (u - u_1)^2}.$$

For this choice of $g_1(u)$ the auxiliary functions $h(u)$ and $f(u)$ can be written explicitly in term of Legendre polynomials. In the limit $\theta \to 0$ we obtain $\lim_{\theta\to 0} g_1(u;\theta) = \delta(u - u_1)$. Then

$$h(u) = 1 \text{ and } f(u) = \begin{cases} 1 \text{ if } u \leq u_1 \\ -1 \text{ if } u > u_1. \end{cases}$$

By using these explicit expressions we can rewrite (4.69) in the form

$$\overline{V} = \frac{1}{2}\left[\int_{-1/2}^{u_1} g_2(u)du - \int_{u_1}^{1/2} g_2(u)du - 2u_1\right]. \tag{4.71}$$

If we now suppose that $g_2(u) = \delta(u - u_2)$ the expression for velocity reduces to

$$\overline{V} = \frac{1}{2}\begin{cases} 1 - 2u_1 \text{ if } u_2 < u_1 \\ -2u_1 \text{ if } u_2 = u_1 \\ -1 - 2u_1 \text{ if } u_2 > u_1 \end{cases}.$$

It is now clear that the velocity reaches its maximal value as $u_1 \to -1/2$ while $u_2 < u_1$. We can then formally write $u_2 = u_1 = -1/2$ and claim that controls $g_2(u) = g_1(u) = \delta(u + 1/2)$ saturate the bound $\overline{V} = 1$. Notice, however, that if we assume directly $u_1 = u_2 \to -1/2$ in (4.71), we obtain $\overline{V} = 1/2$. This is in agreement with the physical intuition that the anchorage point must be located to the right of the pulling force dipole: in this case the pulling forces advance the rear edge of the segment with minimal slipping. Mathematically, we encounter here the case of non-commutation of the limiting procedures $u_2 \to -1/2$, $u_1 \to -1/2$ and we obtain $\overline{V} = 1$ only if the limits are taken in the above order.

To summarize, the optimization of the distribution of focal adhesions allows the contraction-driven segment to reach the value of velocity which is twice as large as when the adhesion is uniform. This means that in order to improve performance, the adhesion must conspire with the contraction machinery making sure that both the motors and the adhesive centers are localized at the trailing edge. Interestingly, exactly this type of correlation between the stresses created by contraction and the distribution of focal adhesions was observed in experiments and numerical simulations [18, 52, 143, 161, 162, 164]. The localization of adhesion complexes close to cell edges, where contraction is the strongest, has been also reported outside the motility context [19, 43, 107].

4.4.3 The General Case

We now turn to the general case where both contraction and protrusion are active. In particular, the protrusive power will be characterized by the parameter $\overline{\Delta V} = T > 0$ which was assumed to be equal to zero in the previous section. In this more general setting we can write

$$\overline{V} = \frac{1}{2}\left[\frac{\int_{-1/2}^{1/2} f(u)du}{\int_{-1/2}^{1/2} h(u)du} T + \int_{-1/2}^{1/2} f(u)(g_2(u) - \hat{g}_2)du\right]. \tag{4.72}$$

As we see, the first term in the right hand side is associated with protrusion-based (filament driven) motility while the second term is the contribution due to contraction-based (motor driven) motility [128]. We notice that if $g_1(u)$ is even, then $f(u)$ is odd and $h(u)$ is even, leading to

$$\frac{\int_{-1/2}^{1/2} f(u)du}{\int_{-1/2}^{1/2} h(u)du} = 0.$$

If $g_2(u)$ is also even, then

$$\int_{-1/2}^{1/2} f(u)(g_2(u) - \hat{g}_2)du = 0.$$

In this case the velocity of the segment is fully controlled by the accretion mechanism characterized by the parameter $\overline{V_m}$.

Consider first the case of protrusion-driven motility by assuming that contraction is homogeneous $g_2(u) \equiv 1$ and therefore does not contribute to the overall velocity. By using again the maximum principle we obtain inequalities

$$-1 \leq \frac{\int_{-1/2}^{1/2} f(u)du}{\int_{-1/2}^{1/2} h(u)du} \leq 1,$$

leading to the upper bound

$$\overline{V} \leq \frac{T}{2}. \tag{4.73}$$

The maximum of the protrusive contribution to velocity is reached when, $g_1(u) = \delta(u-\frac{1}{2})$, because in this case $h = 1$ and $f = 1$ almost everywhere. Observe, that the optimal solution in the case of protrusion-driven motility is in some sense *opposite* to the solution $g_1(u) = \delta(u + 1/2)$ obtained in the case of the contraction-driven motility.

Based on (4.70) and (4.73) we can now argue that in the case when both treadmilling and contraction are present, an upper bound for velocity is

$$\overline{V} \leq \frac{T}{2} + 1.$$

However, in view of the incompatibility of the corresponding optimal controls, this bound cannot be reached. The optimal strategy for focal adhesions would then require a compromise between the necessity to localize adhesion at the trailing edge in order to assist the contraction mechanism and the competing need to localize adhesion at the leading edge in order to improve the protrusion power of the cell.

To obtain a lower bound for $\overline{V}$ we now consider a particular test function representing a weighted sum of our competing optimal controls, $g_1(u) = q\delta(u + 1/2) + (1 - q)\delta(u - 1/2)$. We also chose $g_2(u) = \delta(u - u_0)$, where $q \in [0, 1]$ and $u_0 \in [-1/2, 1/2]$ are two parameters to be optimized. Then, by solving (4.68) we obtain,

$$f(u) = \begin{cases} 1 \text{ if } u = -1/2 \\ \frac{1-2q}{1+q(1-q)L^2} \text{ if } u \in]-1/2, 1/2[\\ -1 \text{ if } u = 1/2 \end{cases}$$

and,

$$h(u) = \begin{cases} 1 \text{ if } u = -1/2 \\ \frac{1}{1+q(1-q)L^2} \text{ if } u \in]-1/2, 1/2[\\ 1 \text{ if } u = 1/2, \end{cases}$$

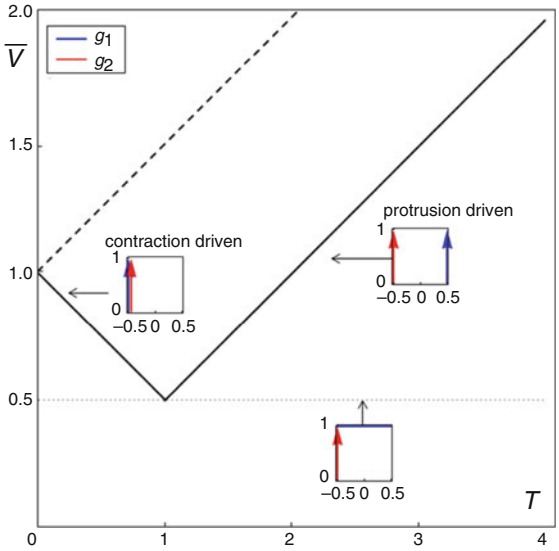

Fig. 4.16 *Solid lines*: lower bound on the optimal velocity of self-propulsion $\overline{V}$ as a function of the measure of the (relative) protrusive strength T. The optimal strategy depends on whether contraction ($T < 1$) or protrusion ($T > 1$) dominates. The *dashed line* represents the upper bound obtained by formally summing the incompatible upper bounds for the protrusion and contraction based strategies. The *dotted line* represents a sub-optimal strategy obtained under the assumption that adhesion is homogeneous. *Insets* illustrate the associated configurations of controls $g_1(u)$ and $g_2(u)$

which leads to the expression for the velocity

$$\overline{V} = \frac{T}{2}(1-2q) + \frac{1}{2}(f(u_0) - (1-2q)h(u_0)).$$

The optimization with respect to u_0 gives $u_0 = -1/2$ and

$$\overline{V} = \frac{T}{2} - q(T-1).$$

Finally, optimizing in q we obtain that if $T < 1$, we must have $q = 0$ and if $T > 1$, we must have $q = 1$. This result, illustrated in Fig. 4.16, suggests that there is a switch at $T = 1$ between the contraction-centered optimization strategy ($q = 0$) and the protrusion-centered optimization strategy ($q = 1$). Notice that the switch takes place exactly when the negative protrusion generated couple T becomes equal to the positive contractile couple equal to 1. At a 'critical' state $T = 1$, the two active mechanisms neutralize each other and active dipoles become invisible behind the passive terms in Eq. (4.64): in this case the optimal position of active agents becomes indeterminate.

To show that the low bound obtained above is rather close to being optimal we solved in [123] the optimization problem numerically. Our numerical results are in full agreement with the analytic bounds. In [123] we also used a perturbation analysis to provide additional evidence that our lower bounds are close to being optimal.

Based on all these studies we conjecture that the function $\overline{V}(T)$, representing the optimal velocity, is piece-wise linear with a kink at $T = 1$. The presence of a threshold indicates a switch from contraction-dominated motility pattern to protrusion-dominated motility pattern. As the relative power of protrusion, epitomized by T, increases beyond this threshold, the focal adhesions, maintaining the optimality of the self-propulsion velocity, must migrate from the trailing to the leading edge of the active segment. The dynamic migration of adhesion proteins to the edges has been observed in experiments [107]. In real cells, however, both edges are usually populated by adhesion complexes and we can speculate that in this way cells can adjust more smoothly to transitions from one driving mode to another.

4.4.4 Discussion

In this section we studied optimal strategies allowing cells to move faster by actively coordinating spatial distributions of contractile and adhesive agents. Our study reveals that if adhesion complexes can detect the dominating mechanism of self propulsion, they can self-organize to ensure the best performance.

We made specific predictions regarding the advantageous correlations between the distributions of adhesive and force producing agents and showed that the dependence of the maximal velocity of self-propulsion on the relative strength of contraction and protrusion may be non-monotone. In particular, our model predicts that a limited activation of protrusion will necessarily lower the maximal velocity achieved in a purely contractile mode of self-propulsion. However, as the protrusion strength increases, protrusion can overtake contraction and the velocity of self-propulsion will increase beyond the level achieved in the contraction-dominated case.

In the first section we saw that contraction-driven motility mechanism may be sufficient to ensure cell polarization, motility initiation, motility arrest and the symmetrization of a cell before mitosis [124, 126]. However, from the analysis presented in the present section it becomes evident that, if the speed of self-propulsion is an issue, cells should mostly rely on protrusion. More specifically, to maximize its velocity performance after motility initiation a cell must switch from contraction-dominated to protrusion-dominated motility mechanism by increasing the protrusive power and appropriately rearranging the distribution of adhesive complexes, see [122] for comparison with experiment. We have seen in the previous section that similar transitions between contraction and protrusion mechanisms can be used by a cell to accommodate different types of cargo.

A schematic nature of the proposed one-dimensional model conceals considerable complexity of the actual cell motility phenomenon which involves intricate bio-chemical feedback loops, geometrically complex mechanical flows and highly nontrivial rheological behavior. In particular, the singular nature of the obtained optimal distributions can be at least partially linked to the fact that polymerization and depolymerization processes are localized at the edges. The situation is complicated further by the fact that the dominant trade-off condition, controlling the self-organization of active agents, is still unknown notwithstanding some recent results in this direction [125]. However, even in the absence of the definitive optimization criterion and with minimal assumptions about the inner working of the motility machinery, our study reveals that depending on the task and the available resources a cell may have to modify its mode of operation rather drastically to ensure the best performance.

4.5 Conclusions

In this chapter we used one-dimensional representations of cellular crawling to illustrate various interactions between the sub-mechanisms of the motility machinery. First, we used a one-dimensional model to expose a crucial role played in cell motility by the nonlocal feedback between contraction and advection and showed that both, motility initiation (implying polarization) and motility arrest (associated with re-symmetrization) may be exclusively contraction-driven. We then demonstrated that a one-dimensional approach presents a unique analytic perspective on the load-induced switching between contraction and protrusion as the dominating motility mechanisms and allows one to trace how different tasks can be accomplished by the structural shifts in motility machinery. Finally, we used a one-dimensional model to provide evidence that radically different spatial distributions of adhesive complexes may be optimal depending on the domineering mechanism of self-propulsion.

While our basic models were rooted in the same theory of active gels we treated contraction-induced active stresses differently in different sections of this chapter. In the first section, focused on contraction proper, we introduced a rather detailed physical model accounting of both force generation and transport of force producing elements. In the second section, where protrusion was the main player, we made a simplifying assumption that the motors are uniformly distributed in the lamellipodium. In the third section aiming at active redistribution of adhesive complexes we did not specify the transport mechanism for contractile elements allowing them to redistribute optimally to ensure that the velocity of directional motility takes the largest value. Some of these assumptions are obviously extreme and have been made with a single purpose of highlighting a particular sub-mechanism of cell motility which would be otherwise obscured by various other contributing factors. However, the unavoidable oversimplifications associated with these assumptions, allowed us to reveals several robust effects:

1. The role played in cell motility by the nonlocal feedback between the mechanics and the transport of active agents.
2. The competition between the dominating driving modes and the possibility of abrupt switches between them depending on the task.
3. A feasibility that the physical mechanism of self-propulsion allows the system to ensure certain optimality of the response.

Despite the overall appeal of the proposed one-dimensional models, they leaves several crucial questions unanswered. Thus, our focus on a normal velocity of self-propulsion obscured the detailed description of the reverse flow of actin monomers which we have replaced with an opaque jump process. Similarly, our desire to maximally limit the number of allowed activity mechanisms, forced us to assume that polymerization of actin monomers and their transport are fast, equilibrium processes. The assumption of infinite compressibility of the cytoskeleton, which is behind the decoupling of the mass transport from the momentum balance, is equally questionable in the light of recent advances in the understanding of cytoskeletal constitutive response [24, 116]. Finally, our schematic depiction of focal adhesions as passive frictional pads needs to be corrected by the account of the ATP driven integrin activity and the mechanical feedback from the binders to the cytoskeleton [138]. These and other simplifications would have to be reconsidered in a richer setting with realistic flow geometry which will also open a way towards more adequate description of the membrane and to account for the polar nature of the gel [55, 96, 152].

Ultimately, the answer to the question whether the proposed simplified description is sufficient to provide the fundamental explanation of the motility initiation and arrest, of the cargo-induced switch between contraction and protrusion and of the adjustment of adhesive mechanism to changes in domineering self-propulsion mode, will depend on the extent to which the inclusion of the factors mentioned above affects our main conclusions. A more thorough analysis will also open the way towards much deeper understanding of each of these effects, in particular, it should be able to explain the remarkable efficiency of the autotaxis mechanism of self-propulsion delivering almost optimal performance at a minimal metabolic cost [125].

Acknowledgements Considerable part of this research was conducted in collaboration with J-F. Joanny and T. Putelat. We thank F. Alouges, D. Ambrosi, O. du Roure, J. Etienne, G. Geymonnat, A. Grosberg, K. Kruse, and C. Verdier for helpful discussions.

References

1. M. Abercrombie, Contact inhibition: the phenomenon and its biological implications. Natl. Cancer Inst. Monogr. **26**, 249 (1967)
2. M. Abercrombie, Croonian lecture, 1978 - crawling movement of metazoan cells (English). Proc. R. Soc. Lond. Ser B Biol. Sci. **207**(1167), 129–147 (1980)

3. Y. Adler, S. Givli, Closing the loop: lamellipodia dynamics from the perspective of front propagation. Phys. Rev. E **88**(4), 042708 (2013)
4. A. Ahmadi, M.C. Marchetti, T.B. Liverpool, Hydrodynamics of isotropic and liquid crystalline active polymer solutions. Phys. Rev. E **74**(6), 061913 (2006)
5. B. Alberts, A. Johnson, J. Lewis, M. Raff, K. Roberts, P. Walter, *Molecular Biology of the Cell*, 4th edn. (Garland Science Taylor & Francis Group, New York, 2002)
6. J. Allard, A. Mogilner, Traveling waves in actin dynamics and cell motility. Curr. Opin. Cell Biol. **25**(1), 107–115 (2013)
7. W. Alt, M. Dembo, Cytoplasm dynamics and cell motion: two-phase flow models. Math. Biosci. **156**(12), 207–228 (1999)
8. S.J. Altschuler, S.B. Angenent, Y. Wang, L.F. Wu, On the spontaneous emergence of cell polarity. Nature **454**(7206), 886–889 (2008)
9. J.C. Amazigo, B. Budiansky, G.F. Carrier, Asymptotic analyses of the buckling of imperfect columns on nonlinear elastic foundations. Int. J. Solids Struct. **6**(10), 1341–1356 (1970)
10. S. Banerjee, M.C. Marchetti, Substrate rigidity deforms and polarizes active gels. Europhys. Lett. **96**(2), 28003 (2011)
11. S. Banerjee, M.C. Marchetti, Contractile stresses in cohesive cell layers on finite-thickness substrates. Phys. Rev. Lett. **109**(10), 108101 (2012)
12. E.L. Barnhart, G.M. Allen, F. Julicher, J.A. Theriot, Bipedal locomotion in crawling cells. Biophys. J. **98**(6), 933–942 (2010)
13. E.L. Barnhart, K.-C. Lee, K. Keren, A. Mogilner, J.A. Theriot, An adhesion-dependent switch between mechanisms that determine motile cell shape. PLoS Biol. **9**(5), e1001059 (2011)
14. E. Barnhart, K.-C. Lee, G.M. Allen, J.A. Theriot, A. Mogilner, Balance between cell-substrate adhesion and myosin contraction determines the frequency of motility initiation in fish keratocytes. PNAS **112**(16), 5045–5050 (2015) published ahead of print April 6, 2015
15. P. Bell, Cell behavior - a tribute to Abercrombie, in ed. by R. Michael - Bellairs, A. Curtis, G. Dunn (English). Am Scientist **72**(1), 88–89 (1984)
16. R. Bellairs, Michael Abercrombie (1912–1979) (English). Int. J. Dev. Biol. **44**(1), 23–28 (2000)
17. A. Bernheim-Groswasser, J. Prost, C. Sykes, Mechanism of actin-based motility: a dynamic state diagram (English). Biophys. J. **89**(2), 1411–1419 (2005)
18. A. Bershadsky, M. Kozlov, B. Geiger, Adhesion-mediated mechanosensitivity: a time to experiment, and a time to theorize. Curr. Opin. Cell Biol. **18**(5), 472–481 (2006)
19. A. Besser, U.S. Schwarz, Coupling biochemistry and mechanics in cell adhesion: a model for inhomogeneous stress fiber contraction. New J. Phys. **9**(11), 425 (2007)
20. C. Blanch-Mercader, J. Casademunt, Spontaneous motility of actin lamellar fragments. Phys. Rev. Lett. **110**(7), 078102 (2013)
21. D. Boal, *Mechanics of the Cell* (Cambridge University Press, Cambridge, 2002)
22. J.S. Bois, F. Jülicher, S.W. Grill, Pattern formation in active fluids. Phys. Rev. Lett. **106**(2), 028103 (2011)
23. D. Bray, *Cell Movements: From Molecules to Motility*, 2nd edn. (Garland Science, New York, 2000)
24. C.P. Broedersz, F.C. MacKintosh, Modeling semiflexible polymer networks. Rev. Mod. Phys. **86**(3), 995–1036 (2014)
25. J. Brugués, J. Casademunt, Self-organization and cooperativity of weakly coupled molecular motors under unequal loading. Phys. Rev. Lett. **102**(11), 118104 (2009)
26. C. Brunner, A. Ehrlicher, B. Kohlstrunk, D. Knebel, J. Ks, M. Goegler, Cell migration through small gaps. Eur. Biophys. J. **35**(8), 713–719 (2006). doi:10.1007/s00249-006-0079-1
27. E. Caglioti, P.L. Lions, C. Marchioro, M. Pulvirenti, A special class of stationary flows for two-dimensional Euler equations: a statistical mechanics description. Commun. Math. Phys. **143**, 501–525 (1992)
28. A.C. Callan-Jones, F. Julicher, Hydrodynamics of active permeating gels. New J. Phys. **13**(9), 093027 (2011). http://stacks.iop.org/1367-2630/13/i=9/a=093027

29. A. Callan-Jones, R. Voituriez, Active gel model of amoeboid cell motility. New J. Phys. **15**(2), 025022 (2013)
30. A.C. Callan-Jones, J.-F. Joanny, J. Prost, Viscous-fingering-like instability of cell fragments. Phys. Rev. Lett. **100**(25), 258106 (2008)
31. V. Calvez, N. Meunier, R. Voituriez, A one-dimensional Keller-Segel equation with a drift issued from the boundary. C. R. Math. **348**(1112), 629–634 (2010)
32. O. Campas, L. Mahadevan, J.-F. Joanny, Actin network growth under load (English). Biophys. J. **102**(5), 1049–1058 (2012)
33. A.E. Carlsson, Mechanisms of cell propulsion by active stresses. New J. Phys. **13**(7), 073009 (2011)
34. A.E. Carlsson, D. Sept, Mathematical modeling of cell migration (English), in *Biophysical Tools for Biologists: Vol 1 In Vitro Techniques*. Methods in Cell Biology, vol. 84 (Elsevier Academic Press Inc, San Diego, 2008), pp. 911+
35. J. Carr, R.L. Pego, Metastable patterns in solutions of ut = e2 uxx - f(u). Commun. Pure Appl. Math. **42**(5), 523–576 (1989)
36. C. Chen, C. Lin, On the symmetry of blowup solutions to a mean field equation. Ann. Inst. Henri Poincare (C) Non Linear Anal. **18**(3), 271–296 (2001) [Elsevier]
37. D.T.N. Chen, Q. Wen, P.A. Janmey, J.C. Crocker, A.G. Yodh, Rheology of soft materials, in *Annual Review of Condensed Matter Physics*, ed. by J.S. Langer, vol. 1 (2010), pp. 301–322. http://www.annualreviews.org/doi/abs/10.1146/annurev-conmatphys-070909-104120
38. B. Cleuren, C. Van den Broeck, Brownian motion with absolute negative mobility (English) Phys. Rev. E **67**(5), Part 2 (2003)
39. B.N. Cox, D.W. Smith, On strain and stress in living cells. J. Mech. Phys. Solids **71**, 239–252 (2014)
40. G. Csucs, K. Quirin, G. Danuser, Locomotion of fish epidermal keratocytes on spatially selective adhesion patterns. Cell Motil. Cytoskeleton **64**(11), 856–867 (2007)
41. A.T. Dawes, G.B. Ermentrout, E.N. Cytrynbaum, L. Edelstein-Keshet, Actin filament branching and protrusion velocity in a simple 1D model of a motile cell. J. Theor. Biol. **242**(2), 265–279 (2006)
42. S.R. De Groot, P. Mazur, *Non-Equilibrium Thermodynamics* (Courier Dover Publications, New York, 2013)
43. V.S. Deshpande, M. Mrksich, R.M. McMeeking, A.G. Evans, A bio-mechanical model for coupling cell contractility with focal adhesion formation (English). J. Mech. Phys. Solids **56**(4), 1484–1510 (2008)
44. P. DiMilla, K. Barbee, D. Lauffenburger, Mathematical-model for the effects of adhesion and mechanics on cell-migration speed (English). Biophys. J. **60**(1), 15–37 (1991)
45. E. Doedel, A. Champneys, F. Dercole, T. Fairgrieve, Y.A. Kuznetsov, B. Oldeman, R. Paffenroth, B Sandstede, X. Wang, C. Zhang, AUTO-07p, in *Continuation and Bifurcation Software for Ordinary Differential Equations* (2007). Available at http://cmvl.cs.concordia.ca/auto
46. K. Doubrovinski, K. Kruse, Self-organization of treadmilling filaments. Phys. Rev. Lett. **99**(22), 228104 (2007)
47. K. Doubrovinski, K. Kruse, Self-organization in systems of treadmilling filaments (English). Eur. Phys. J. E **31**(1), 95–104 (2010)
48. K. Doubrovinski, K. Kruse, Cell motility resulting from spontaneous polymerization waves. Phys. Rev. Lett. **107**(25), 258103 (2011)
49. X. Du, K. Doubrovinski, M. Osterfield, Self-organized cell motility from motor-filament interactions. Biophys. J. **102**(8), 1738–1745 (2012)
50. J. Étienne, D. Mitrossilis, J. Fouchard, N. Bufi, P. Durand-Smet, A. Asnacios, Collective dynamics of actomyosin cortex endow cells with intrinsic mechanosensing properties. arXiv preprint. arXiv:1407.2765, accepted in PNAS (2014)
51. B. Finlayson, L. Scriven, Convective instability by active stress. Proc. R. Soc. Lond. A. Math. Phys. Sci. **310**(1501), 183–219 (1969)

52. H. Gao, J. Qian, B. Chen, Probing mechanical principles of focal contacts in cell-matrix adhesion with a coupled stochastic-elastic modelling framework. J. R. Soc. Interface **8**(62), 1217–1232 (2011)
53. M.L. Gardel, B. Sabass, L. Ji, G. Danuser, U.S. Schwarz, C.M. Waterman, Traction stress in focal adhesions correlates biphasically with actin retrograde flow speed. J. Cell Biol. **183**(6), 999–1005 (2008)
54. M.L. Gardel, I.C. Schneider, Y. Aratyn-Schaus, C.M. Waterman, Mechanical integration of actin and adhesion dynamics in cell migration, in *Annual Review of Cell and Developmental Biology*, ed. by R. Schekman, L. Goldstein, R. Lehmann, vol. 26. (2010), pp. 315–333. http://www.annualreviews.org/doi/abs/10.1146/annurev.cellbio.011209.122036
55. L. Giomi, A. DeSimone, Spontaneous division and motility in active nematic droplets. Phys. Rev. Lett. **112**(14), 147802 (2014)
56. F. Gladiali, M. Grossi, H. Ohtsuka, T. Suzuki, Morse indices of multiple blow-up solutions to the two-dimensional Gel'fand problem. arXiv preprint arXiv:1210.1373 (2012)
57. P. Haenggi, F. Marchesoni, S. Savel'ev, G. Schmid, Asymmetry in shape causing absolute negative mobility (English). Phys. Rev. E **82**(4), Part 1 (2010)
58. R.J. Hawkins, R. Voituriez, Mechanisms of cell motion in confined geometries. Math. Model. Nat. Phenom. **5**(1), 84–105 (2010)
59. R.J. Hawkins, O. Bénichou, M. Piel, R. Voituriez, Rebuilding cytoskeleton roads: Active-transport-induced polarization of cells. Phys. Rev. E Stat. Nonlinear Soft Matter Phys. **80**(4), 040903+ (2009)
60. R.J. Hawkins, M. Piel, G. Faure-Andre, A.M. Lennon-Dumenil, J.F. Joanny, J. Prost, R. Voituriez, Pushing off the walls: a mechanism of cell motility in confinement (English). Phys. Rev. Lett. **102**(5), 058103 (2009)
61. R.J. Hawkins, R. Poincloux, O. Benichou, M. Piel, P. Chavrier, R. Voituriez, Spontaneous contractility-mediated cortical flow generates cell migration in three-dimensional environments. Biophys. J. **101**(5), 1041–1045 (2011)
62. C.A. Heckman, Contact inhibition revisited. J. Cellular Physiol. **220**(3), 574–575 (2009)
63. M. Herant, M. Dembo, Form and function in cell motility: from fibroblasts to keratocytes. Biophys. J. **98**(8), 1408–1417 (2010)
64. N. Hodge, P. Papadopoulos, Continuum modeling and numerical simulation of cell motility. J. Math. Biol. **64**(7), 1253–1279 (2012)
65. B.D. Hoffman, J.C. Crocker, Cell mechanics: dissecting the physical responses of cells to force. Annu. Rev. Biomed. Eng. **11**, 259–288 (2009)
66. J. Howard, *Mechanics of Motor Proteins and the Cytoskeleton* (Sinauer Associates, Sunderland, 2001)
67. J. Howard, S.W. Grill, J.S. Bois, Turing's next steps: the mechanochemical basis of morphogenesis. Nat. Rev. Mol. Cell Biol. **12**(6), 392–398 (2011)
68. E.-M. Hur, I.H. Yang, D.-H. Kim, J. Byun, W.-L. Xu, P.R. Nicovich, R. Cheong, A. Levchenko, N. Thakor, F.-Q. Zhou, et al., Engineering neuronal growth cones to promote axon regeneration over inhibitory molecules. Proc. Natl. Acad. Sci. **108**(12), 5057–5062 (2011)
69. H. Jiang, S.X. Sun, Cellular pressure and volume regulation and implications for cell mechanics. Biophys. J. **105**(3), 609–619 (2013)
70. A. Jilkine, L. Edelstein-Keshet, A comparison of mathematical models for polarization of single eukaryotic cells in response to guided cues. PLoS Comput. Biol. **7**(4), e1001121 (2011)
71. J.-F. Joanny, J. Prost, Constructing tools for the description of cell dynamics, in *Biological Physics: Poincare Seminar 2009*, ed. by B. Duplantier, V. Rivasseau. Progress in Mathematical Physics, vol. 60. 12th Poincare Seminar on Biological Physics, Inst Henri Poincare, Paris, Jan 31, 2009. Commissariat Energie Atomique, Div Sci Matiere; Daniel Iagolnitzer Fdn; Ecole Polytechnique (2011), pp. 1–32
72. J. Joanny, F. Julicher, J. Prost, Motion of an adhesive gel in a swelling gradient: a mechanism for cell locomotion (English). Phys. Rev. Lett. **90**(16), 168102 (2003)
73. J.F. Joanny, F. Julicher, K. Kruse, J. Prost, Hydrodynamic theory for multi-component active polar gels (English). New J. Phys. **9**(11), 422 (2007)

74. K. John, P. Peyla, K. Kassner, J. Prost, C. Misbah, Nonlinear study of symmetry breaking in actin gels: implications for cellular motility. Phys. Rev. Lett. **100**(6), 068101 (2008)
75. F. Julicher, K. Kruse, J. Prost, J.-F. Joanny, Active behavior of the cytoskeleton (English). Phys. Rep. Rev. Section Phys. Lett. **449**(1–3), 3–28 (2007)
76. H. Keller, A.D. Zadeh, P. Eggli, Localised depletion of polymerised actin at the front of Walker carcinosarcoma cells increases the speed of locomotion. Cell Motil. Cytoskeleton **53**(3), 189–202 (2002)
77. L. Kimpton, J. Whiteley, S. Waters, J. Oliver, On a poroviscoelastic model for cell crawling. J. Math. Biol. **70**(1), 133–171 (2015)
78. W. Koiter, *Current Trends in the Theory of Buckling* (Springer, Berlin, 1976)
79. K. Kruse, F. Julicher, Actively contracting bundles of polar filaments. Phys. Rev. Lett. **85**(8), 1778–1781 (2000)
80. K. Kruse, F. Jülicher, Self-organization and mechanical properties of active filament bundles. Phys. Rev. E **67**(5), 051913 (2003)
81. K. Kruse, A. Zumdieck, F. Jlicher, Continuum theory of contractile fibres. Europhys. Lett. **64**(5), 716 (2003)
82. K. Kruse, J. Joanny, F. Julicher, J. Prost, K. Sekimoto, Generic theory of active polar gels: a paradigm for cytoskeletal dynamics (English). Eur. Phys. J. E **16**(1), 5–16 (2005)
83. K. Kruse, J.F. Joanny, F. Julicher, J. Prost, Contractility and retrograde flow in lamellipodium motion (English). Phys. Biol. **3**(2), 130–137 (2006)
84. O.M. Lancaster, B. Baum, Shaping up to divide: coordinating actin and microtubule cytoskeletal remodelling during mitosis. Semin. Cell Dev. Biol. **34**(0), 109–115 (2014)
85. O.M. Lancaster, M.L. Berre, A. Dimitracopoulos, D. Bonazzi, E. Zlotek- Zlotkiewicz, R. Picone, T. Duke, M. Piel, B. Baum, Mitotic rounding alters cell geometry to ensure efficient bipolar spindle formation. Dev. Cell **25**(3), 270–283 (2013)
86. K. Larripa, A. Mogilner, Transport of a 1D viscoelastic actin-myosin strip of gel as a model of a crawling cell (English). Physica A-Stat. Mech. Appl. **372**(1) (2006). Workshop on Common Trends in Traffic Systems, Kanpur, Feb 08–10, 2006, pp. 113–123
87. E. Lauga, T.R. Powers, The hydrodynamics of swimming microorganisms (English). Rep. Progr. Phys. **72**(9), 096601 (2009)
88. Y. Lin, A model of cell motility leading to biphasic dependence of transport speed on adhesive strength. J. Mech. Phys. Solids **58**(4), 502–514 (2010)
89. Y. Lin, M. Inamdar, L. Freund, The competition between Brownian motion and adhesion in soft materials. J. Mech. Phys. Solids **56**(1), 241–250 (2008)
90. Z. Liu, L. A. van Grunsven, E. Van Rossen, B. Schroyen, J.-P. Timmermans, A. Geerts, H. Reynaert, Blebbistatin inhibits contraction and accelerates migration in mouse hepatic stellate cells. Br. J. Pharmacol. **159**(2), 304–315 (2010)
91. J. Löber, F. Ziebert, I.S. Aranson, Modeling crawling cell movement on soft engineered substrates. Soft Matter **10**(9), 1365–1373 (2014)
92. M.L. Lombardi, D.A. Knecht, M. Dembo, J. Lee, Traction force microscopy in Dictyostelium reveals distinct roles for myosin II motor and actin-crosslinking activity in polarized cell movement. J. Cell Sci. **120**(Pt 9), 1624–1634 (2007)
93. A.J. Loosley, J.X. Tang, Stick-slip motion and elastic coupling in crawling cells. Phys. Rev. E **86**(3), Part 1 (2012)
94. L. Machura, M. Kostur, P. Talkner, J. Luczka, P. Haenggi, Absolute negative mobility induced by thermal equilibrium fluctuations (English). Phys. Rev. Lett. **98**(4), 040601 (2007)
95. M.C. Marchetti, J.-F. Joanny, S. Ramaswamy, T.B. Liverpool, J. Prost, M. Rao, R. Aditi Simha, Soft active matter. (2012). ArXiv e-prints. arXiv:1207.2929 [cond-mat.soft]
96. M. Marchetti, J. Joanny, S. Ramaswamy, T. Liverpool, J. Prost, M. Rao, R.A. Simha, Hydrodynamics of soft active matter. Rev. Mod. Phys. **85**(3), 1143 (2013)
97. M. Mayer, M. Depken, J.S. Bois, F. Julicher, S.W. Grill, Anisotropies in cortical tension reveal the physical basis of polarizing cortical flows. Nature **467**(7315), 617–U150 (2010)
98. G. Meurant, A review on the inverse of symmetrical tridiagonal and block tridiagonal matrices (English). SIAM J. Matrix Anal. Appl. **13**(3), 707–728 (1992)

99. Q. Mi, D. Swigon, B. Riviere, S. Cetin, Y. Vodovotz, D.J. Hackam, One-dimensional elastic continuum model of enterocyte layer migration (English). Biophys. J. **93**(11), 3745–3752 (2007)
100. S. Mikhlin, *Linear Integral Equations* (Hindustan Publishing Corp., DELHI (India) 1960)
101. M.R.K. Mofrad, Rheology of the cytoskeleton. Ann. Rev. Fluid Mech. **41**, 433–453 (2009)
102. A. Mogilner, Mathematics of cell motility: have we got its number? (English). J. Math. Biol. **58**(1–2) (2009). International Conference on Industrial and Applied Mathematics (Zurich, 2007), pp. 105–134
103. A. Mogilner, L. Edelstein-Keshet, Regulation of actin dynamics in rapidly moving cells: a quantitative analysis (English). Biophys. J. **83**(3), 1237–1258 (2002)
104. Y. Mori, A. Jilkine, L. Edelstein-Keshet, Wave-pinning and cell polarity from a bistable reaction-diffusion system. Biophys. J. **94**(9), 3684–3697 (2008)
105. C. Nelson, Paluch, Ewa K, Nelson, Celeste M, Biais, Nicolas, Fabry, Ben, Moeller, Jens, Pruitt, Beth L, Wollnik, Carina, Kudryasheva, Galina and Rehfeldt, Florian, Federle, Walter, Mechanotransduction: use the force (s). BMC Biol., BioMed Central Ltd **13**(1), 47 (2015). http://www.biomedcentral.com/1741-7007/13/47
106. L. Nirenberg, *Topics in Nonlinear Functional Analysis*, vol. 6 (American Mathematical Society, Providence, RI, 1974)
107. I.L. Novak, B.M. Slepchenko, A. Mogilner, L.M. Loew, Cooperativity between cell contractility and adhesion. Phys. Rev. Lett. **93**(26), 268109 (2004)
108. H. Ohtsuka, A concentration phenomenon around a shrinking hole for solutions of mean field equations. Osaka J. Math. **39**, 395–407 (2002)
109. J. Oliver, J. King, K. McKinlay, P. Brown, D. Grant, C. Scotchford, J. Wood, Thin-film theories for two-phase reactive flow models of active cell motion. Math. Med. Biol. **22**(1), 53–98 (2005)
110. J.G. Orlandi, C. Blanch-Mercader, J. Brugués, J. Casademunt, Cooperativity of self-organized Brownian motors pulling on soft cargoes. Phys. Rev. E **82**(6), 061903 (2010)
111. A. Pathak, V.S. Deshpande, R.M. McMeeking, A.G. Evans, The simulation of stress fibre and focal adhesion development in cells on patterned substrates (English). J. R. Soc. Interface **5**(22), 507–524 (2008)
112. B. Perthame, *Growth, Reaction, Movement and Diffusion from Biology*. Lecture Notes, University Paris **6** (2012)
113. C. Peskin, G. Odell, G. Oster, Cellular motions and thermal fluctuations - the Brownian ratchet (English). Biophys. J. **65**(1), 316–324 (1993)
114. R. Poincloux, O. Collin, F. Lizárraga, M. Romao, M. Debray, M. Piel, P. Chavrier, Contractility of the cell rear drives invasion of breast tumor cells in 3D Matrigel. Proc. Natl. Acad. Sci. U.S.A. **108**(5), 1943–1948 (2011)
115. M. Prass, K. Jacobson, A. Mogilner, M. Radmacher, Direct measurement of the lamellipodial protrusive force in a migrating cell. J. Cell Biol. **174**, 767–772 (2006)
116. R.H. Pritchard, Y.Y. Shery Huang, E.M. Terentjev, Mechanics of biological networks: from the cell cytoskeleton to connective tissue. Soft Matter **10**(12), 1864–1884 (2014)
117. J. Prost, C. Barbetta, J.-F. Joanny, Dynamical control of the shape and size of Stereocilia and Microvilli. Biophys. J. **93**(4), 1124–1133 (2007)
118. J. Prost, F. Jülicher, J. Joanny, Active gel physics. Nat. Phys. **11**(2), 111–117 (2015)
119. E.M. Purcell, Life at low Reynolds number. Am. J. Phys. **45**(1), 3–11 (1977)
120. S. Rafelski, J. Theriot, Crawling toward a unified model of cell motility: spatial and temporal regulation of actin dynamics (English). Ann. Rev. Biochem. **73**, 209–239 (2004)
121. J. Ranft, J. Prost, F. Jülicher, J.-F. Joanny, Tissue dynamics with permeation. Eur. Phys. J. E. Soft Matter **35**, 9723 (2012)
122. P. Recho, L. Truskinovsky, Asymmetry between pushing and pulling for crawling cells. Phys. Rev. E **87**(2), 022720 (2013)
123. P. Recho, L. Truskinovsky, Maximum velocity of self-propulsion for an active segment. Math. Mech. Solids (2015). http://mms.sagepub.com/content/early/2015/07/06/1081286515588675.abstract

124. P. Recho, T. Putelat, L. Truskinovsky, Contraction-driven cell motility. Phys. Rev. Lett. **111**(10), 108102 (2013)
125. P. Recho, J.-F. Joanny, L. Truskinovsky, Optimality of contraction-driven crawling. Phys. Rev. Lett. **112**(21), 218101 (2014)
126. P. Recho, T. Putelat, L. Truskinovsky, Mechanics of motility initiation and motility arrest in crawling cells. J. Mech. Phys. Solids **84**, 469–505 (2015). Doi:http://dx.doi.org/10.1016/j.jmps.2015.08.006. Available at http://www.sciencedirect.com/science/article/pii/S0022509615300612
127. A.J. Ridley, M.A. Schwartz, K. Burridge, R.A. Firtel, M.H. Ginsberg, G. Borisy, J.T. Parsons, A.R. Horwitz, Cell migration: integrating signals from front to back. Science **302**(5651), 1704–1709 (2003). eprint: http://www.sciencemag.org/content/302/5651/1704.full.pdf
128. T. Risler, Cytoskeleton and cell motility. (2011). arXiv:1105.2423 [physics.bio-ph]
129. W. Ronan, V.S. Deshpande, R.M. McMeeking, J.P. McGarry, Cellular contractility and substrate elasticity: a numerical investigation of the actin cytoskeleton and cell adhesion. Biomech. Model. Mechanobiol. **13**(2), 417–435 (2014)
130. A. Ros, R. Eichhorn, J. Regtmeier, T. Duong, P. Reimann, D. Anselmetti, Brownian motion - absolute negative particle mobility (English). Nature **436**(7053), 928 (2005)
131. B. Rubinstein, M.F. Fournier, K. Jacobson, A.B. Verkhovsky, A. Mogilner, Actin-myosin viscoelastic flow in the keratocyte lamellipod (English). Biophys. J. **97**(7), 1853–1863 (2009)
132. D. Saintillan, M.J. Shelley, Emergence of coherent structures and large-scale flows in motile suspensions. J. R. Soc. Interface **9**(68), 571–585 (2012)
133. G. Salbreux, J. Prost, J.F. Joanny, Hydrodynamics of cellular cortical flows and the formation of contractile rings. Phys. Rev. Lett. **103**(5), 058102 (2009)
134. S. Sankararaman, S. Ramaswamy, Instabilities and waves in thin films of living fluids. Phys. Rev. Lett. **102**(11), 118107 (2009)
135. C.H. Schreiber, M. Stewart, T. Duke, Simulation of cell motility that reproduces the force-velocity relationship (English). Proc. Natl. Acad. Sci. U.S.A. **107**(20), 9141–9146 (2010)
136. U.S. Schwarz, M.L. Gardel, United we stand - integrating the actin cytoskeleton and cell-matrix adhesions in cellular mechanotransduction. J. Cell Science **125**(13), 3051–3060 (2012)
137. U. Schwarz, S. Safran, Elastic interactions of cells. Phys. Rev. Lett. **88**(4), 048102 (2002)
138. U. Schwarz, S. Safran, Physics of adherent cells. Rev. Mod. Phys. **85**(3), 1327–1381 (2013)
139. J. Sedzinski, M. Biro, A. Oswald, J.-Y. Tinevez, G. Salbreux, E. Paluch, Polar actomyosin contractility destabilizes the position of the cytokinetic furrow. Nature **476**(7361), 462–466 (2011)
140. T. Senba, T. Suzuki, Some structures of the solution set for a stationary system of chemotaxis. Adv. Math. Sci. Appl. **10**(1), 191–224 (2000)
141. D. Shao, W.-J. Rappel, H. Levine, Computational model for cell morphodynamics (English). Phys. Rev. Lett. **105**(10), 108104 (2010)
142. M. Sheetz, J. Sable, H. Dobereiner, Continuous membrane-cytoskeleton adhesion requires continuous accommodation to lipid and cytoskeleton dynamics. Ann. Rev. Biophys. Biomol. Struct. **35**, 417–434 (2006)
143. M. Shutova, C. Yang, J.M. Vasiliev, T. Svitkina, Functions of non-muscle myosin II in assembly of the cellular contractile system. PLoS One **7**(7), e40814–e40814 (2012)
144. R. Simha, S. Ramaswamy, Hydrodynamic fluctuations and instabilities in ordered suspensions of self-propelled particles. Phys. Rev. Lett. **89**(5), 058101_1–058101_4 (2002)
145. M.P. Stewart, J. Helenius, Y. Toyoda, S.P. Ramanathan, D.J. Muller, A.A. Hyman, Hydrostatic pressure and the actomyosin cortex drive mitotic cell rounding. Nature **469**(7329), 226–230 (2011)
146. T. Stossel, On the crawling of animal-cells (English). Science **260**(5111), 1086–1094 (1993)
147. K.M. Stroka, H. Jiang, S.-H. Chen, Z. Tong, D. Wirtz, S.X. Sun, K. Konstantopoulos, Water permeation drives tumor cell migration in confined microenvironments. Cell **157**(3), 611–623 (2014)
148. M. Struwe, G. Tarantello, On multivortex solutions in Chern-Simons gauge theory. Bollettino della Unione Matematica Italiana-B **1**, 109–122 (1998)

149. K. Tawada, K. Sekimoto, Protein friction exerted by motor enzymes through a weak-binding interaction. J. Theor. Biol. **150**(2), 193–200 (1991)
150. T. Thoresen, M. Lenz, M.L. Gardel, Reconstitution of contractile actomyosin bundles. Biophys. J. **100**(11), 2698–2705 (2011)
151. J.-Y. Tinevez, U. Schulze, G. Salbreux, J. Roensch, J.-F. Joanny, E. Paluch, Role of cortical tension in bleb growth. Proc. Natl. Acad. Sci. **106**(44), 18581–18586 (2009)
152. E. Tjhung, A. Tiribocchi, D. Marenduzzo, M. Cates, A minimal physical model captures the shapes of crawling cells. Nat. Commun. **6** (2015)
153. E. Tjhung, D. Marenduzzo, M.E. Cates, Spontaneous symmetry breaking in active droplets provides a generic route to motility. Proc. Natl. Acad. Sci. U.S.A. **109**(31), 12381–12386 (2012)
154. P.G. Torres, K. Doubrovinski, K. Kruse, Filament turnover stabilizes contractile cytoskeletal structures. Europhys. Lett. **91**(6), 68003 (2010)
155. X. Trepat, M.R. Wasserman, T.E. Angelini, E. Millet, D.A. Weitz, J.P. Butler, J.J. Fredberg, Physical forces during collective cell migration. Nat. Phys. **5**(6), 426–430 (2009)
156. H. Turlier, B. Audoly, J. Prost, J.-F. Joanny, Furrow constriction in animal cell cytokinesis. Biophys. J. **106**(1), 114–123 (2014)
157. B. Vanderlei, J.J. Feng, L. Edelstein-Keshet, A computational model of cell polarization and motility coupling mechanics and biochemistry. Multiscale Model. Simul. **9**(4), 1420–1443 (2011)
158. S.R.K. Vedula, M.C. Leong, T.L. Lai, P. Hersen, A.J. Kabla, C.T. Lim, B. Ladoux, Emerging modes of collective cell migration induced by geometrical constraints. Proc. Natl. Acad. Sci. U.S.A. **109**, 12974–12979 (2012)
159. A. Verkhovsky, T. Svitkina, G. Borisy, Self-polarization and directional motility of cytoplasm. Curr. Biol. **9**(1), 11–20 (1999)
160. M. Vicente-Manzanares, D. Webb, A. Horwitz, Cell migration at a glance (English). J. Cell Sci. **118**(21), 4917–4919 (2005)
161. M. Vicente-Manzanares, X. Ma, R.S. Adelstein, A.R. Horwitz, Non-muscle myosin II takes centre stage in cell adhesion and migration. Nat. Rev. Mol. Cell Biol. **10**(11), 778–790 (2009)
162. Y. Wang, E. Botvinick, Y. Zhao, M. Berns, S Usami, R. Tsien, S Chien, Visualizing the mechanical activation of Src. Nature **434**(7036), 1040–1045 (2005)
163. Q. Wang, X. Yang, D. Adalsteinsson, T.C. Elston, K. Jacobson, M. Kapustina, M.G. Forest, Computational and modeling strategies for cell motility, in *Biological and Medical Physics, Biomedical Engineering*, ed. by N.V. Dokholyan (Springer, Heidelberg, 2012), pp. 257–296
164. H. Wolfenson, Y.I. Henis, B. Geiger, A.D. Bershadsky, The heel and toe of the cell's foot: a multifaceted approach for understanding the structure and dynamics of focal adhesions. Cell Motil. Cytoskeleton **66**(11), 1017–1029 (2009)
165. C. Wolgemuth, Lamellipodial contractions during crawling and spreading. Biophys. J. **89**(3), 1643–1649 (2005)
166. C.W. Wolgemuth, J. Stajic, A. Mogilner, Redundant mechanisms for stable cell locomotion revealed by minimal models. Biophys. J. **101**(3), 545–553 (2011)
167. P.T. Yam, C.A. Wilson, L. Ji, B. Hebert, E.L. Barnhart, N.A. Dye, P.W. Wiseman, G. Danuser, J.A. Theriot, Actin-myosin network reorganization breaks symmetry at the cell rear to spontaneously initiate polarized cell motility. J. Cell Biol. **178**(7), 1207–1221 (2007)
168. F. Ziebert, I.S. Aranson, Effects of adhesion dynamics and substrate compliance on the shape and motility of crawling cells. PloS One **8**(5), e64511 (2013)
169. F. Ziebert, S. Swaminathan, I.S. Aranson, Model for self-polarization and motility of keratocyte fragments. J. R. Soc. Interface **9**(70), 1084–1092 (2012)
170. J. Zimmermann, C. Brunner, M. Enculescu, M. Goegler, A. Ehrlicher, J. Kaes, M. Falcke, Actin filament elasticity and retrograde flow shape the force-velocity relation of motile cells. Biophys. J. **102**(2), 287–295 (2012)